Decoding the Eastward Tilt of the Indian Peninsular Plateau: Insights from Geodynamic Modelling

Joyjeet Sen[1], Arnab Roy[2], Nibir Mandal[1*]
[1]Department of Geological Sciences, Jadavpur University, Kolkata 700032, India
[2]Department of Earth and Spatial Sciences, University of Idaho, Moscow 83844, USA
***Corresponding author: nibir.mandal@jadavpuruniversity.in**

Abstract

The eastward tilting of the Indian Peninsular (IP) plateau has been a topic of ongoing debate in geoscience. This study introduces a fresh geodynamic perspective, employing extensive topographic analyses to identify the mechanisms behind this tilting. By analyzing the eastward-flowing river systems in relation to the plateau's tilt, we constructed a series of east-west topographic profiles using digital elevation models (DEM). Our findings indicate a systematic increase in eastward slopes (θ = 0.008° to 0.3°) from the northern boundary to the southern tip of the plateau. Large-scale thermo-mechanical simulations reveal that the configuration of the Indian plate plays a crucial role in driving this tilt. Specifically, we observe that the older lithosphere beneath the Bay of Bengal (age ~ 140 Ma) has subsided at a significantly faster rate than the younger lithosphere beneath the Arabian Sea (age ~ 60 Ma). This differential subsidence has generated westward sub-lithospheric flows beneath the Indian Peninsula, interacting with east-directed mantle flows originating from regions below the Arabian lithosphere. This interaction has resulted in a localized mantle upwelling at the Western IP margin, contributing to the Western Ghats Escarpment (WGE) formation. Furthermore, we examine spatial variations in sub-lithospheric flow patterns to account for the increasing θ towards the south. Our findings suggest that the eastward topographic tilt of the IP is predominantly influenced by sub-lithospheric mantle dynamics, driven by lithospheric density contrasts between the Bay of Bengal and the Arabian Sea. This study provides valuable insights into the drainage patterns in IP.

Key words: Indian Peninsular rivers, Continental-scale topography, Western Ghat Escarpment, Thermomechanical modelling, Sub-lithospheric flow dynamics, Mantle upwelling

1 Introduction

Surface topography and associated drainage patterns in continents result from a combination of endogenous (e.g., crustal deformations) and exogenous (e.g., surface erosion) Earth processes, which operate across a wide range of geological time scales (from thousands to millions of years). These processes typically manifest in large-scale, first-order physiographic features with distinctive river systems, as observed in Peninsular India (IP) (Figure 1). Understanding how topography responds to tectonic forces is thus a crucial step in interpreting the surface architecture of large continents like India that controls their long-term landscape evolution, drainage patterns, and sediment accumulation in basins (Bishop, 2007; Ellis et al., 1999; Kirby & Whipple, 2012; Mandal et al., 2015; Minár et al., 2020; Ruetenik et al., 2016; Stolar et al., 2007; Tucker, 2015; Tucker & Hancock, 2010; Whipple & Meade, 2004; Whipple, 2009). Recent studies have developed various tectonic models to explain the major continental-scale topographic elements, such as mountain ranges, elevated plateaus, foreland basins, fore-arcs, and deep oceanic trenches, as surface expressions of plate kinematics. A well-established example is the Tibetan Plateau, one of Earth's most significant planetary features, which has grown as a result of the India-Asia convergence, attaining an average elevation of about 5 km (DeCelles et al., 2007; Ding et al., 2022; Fang et al., 2020; Maiti et al., 2021). This convergence also led to the rise of the Himalayan Mountain range, setting in a southward topographic slope of approximately 3° in the extra-Peninsular region of India (Copley & Mckenzie, 2007; Houseman & England, 1993; Mandal et al., 2015). While substantial progress has taken place in tectonic modeling of the Himalaya-Tibet Mountain system, the vast Peninsular Plateau, covering much of the southern part of India, has remained largely unexplored from a geodynamical perspective. This plateau lies in a tectonically stable region, as indicated by the low frequency of seismic activity in the present day as well as geologically recent past (Asish et al., 2016; Chandra, 1977; Jaiswal & Sinha, 2007; Rao & Rao, 1984). Its geographical features: a pronounced eastward topographic slope and a predominant eastward drainage flow, present an intriguing scenario (Figure 1). Interestingly, the eastward surface slope appears largely independent of the N-S India-Asia convergence tectonics. The origin of this continental-scale topographic tilt remains unclear, although several hypotheses, diverse in their conceptual frameworks, have been proposed (Campanile et al., 2008; Collier et al., 2008; Cox, 1989; Gunnell & Fleitout, 1998; Kailasam, 1975; Mandal et al., 2015; Pandey et al., 1996; Radhakrishna, 1993; Richards et al., 2016;

Valdiya, 2001; Vita-Finzi, 2004; Watts & Cox, 1989; White & McKenzie, 1989; Whiting et al., 1994).

The distinctive asymmetric topography of the Indian peninsular plateau has sparked an ongoing debate, primarily focused on its age and the factors responsible for the persistent eastward slope. One of the most influential propositions in this discussion claims that the Western Ghats escarpment is the remnant of a past rifting and magmatic event around 65 million years ago, which subsequently formed a passive continental margin that presently defines the ~1600 km long Western boundary of the Peninsular Indian landmass (Cox, 1989; Pandey et al., 1996; White & McKenzie, 1989). In contrast, an alternative perspective, grounded in tectonic evidence, attributes the current asymmetric physiography to more recent neotectonic activities (Valdiya, 2001; Vita-Finzi, 2004). Continued efforts for exploring the mechanisms of this landscape topography deepen the intriguing issues further. Some authors have proposed a flexural response model, claiming that the elevation at the western coastline could be a consequence of combined onshore denudation and offshore sedimentary loading (Campanile et al., 2008; Gunnell et al., 2003; Gunnell & Fleitout, 1998; White & McKenzie, 1989; Whiting et al., 1994). Another hypothesis posits that regional epirogenic uplift, driven by thermal anomalies in the convecting mantle, could be a significant factor (Kailasam, 1975; Radhakrishna, 1993; Richards et al., 2016). These competing theories lead to differing views on the temporal and spatial dimensions of uplift and tilting, though none provide a comprehensive explanation that aligns with the broader geodynamic context of peninsular India.

The problem of the eastwardly tilted peninsular topographic development, with an about 1,500 meters elevation at the Western Ghats escarpment (Richards et al., 2016), opened up geodynamic studies from the perspective of Indian plate reconstructions. From residual depth anomaly measurements, it has been shown that the tilt extends into the adjacent oceanic part of the plate, resulting in residual depths at the east lower than that at the west (Hoggard et al., 2016; Richards et al., 2016). This analysis finds this tilt as a remarkably long-wavelength topographic feature extending over 2,000 kilometers. Cox (1989) suggested that the long-wavelength topography and its resulting drainage pattern in the Indian subcontinent took their shapes during the Paleogene era when the Seychelles region separated from the western margin, potentially due to a mantle plume. However, more recent data suggest that any elevated terrain formed during the Deccan volcanic activity likely underwent rapid denudation, leading to a much-reduced topographic relief by the beginning of the Neogene period (Dole et al., 2022). During the Eocene and Oligocene epochs, extensive lateritic deposits were formed along both the continental margins, as reported by (Bonnet et al., 2014, 2016) and others. This laterite formation, in conjunction with evidence from paleoclimatic studies, points to a low-relief, wet, and tropical climate in peninsular India during this time (Chatterjee et al., 2013; Kent & Muttoni, 2008; Thorne et al., 2012). These findings are further supported by shifts in laterite formation patterns and sedimentation types, suggesting the denudation event approximately 23 million years ago(Raju, 2008). An alternative hypothesis accounts for the relative horizontal motion between the Indian plate and its underlying mantle as a possible factor controlling the long-wavelength tilting. Notably, some studies (Morgan & Smith, 1992; Russo & Silver, 1994) demonstrate the role of subducting slab-driven westward return flows in the asthenosphere (Becker, 2017), covering 2,000 kilometers from the Sunda trench at the eastern extremity of the Indian plate(Steckler et al., 2016). This proposition is supported by station-averaged SKS splits (Becker et al., 2012), claiming that an SSW-directed asthenospheric flow sets in the topographic gradient in peninsular India. In contrast, several geophysical studies report NNE-SSW oriented seismic mantle anisotropy, which is interpreted to be a consequence of the northward mantle flow beneath peninsular India (Heintz et al., 2009; Illa et al., 2021; Kumar et al., 2015; Mandal, 2011; Roy et al., 2024; Roy et al., 2012). This kinematic condition, however, appears to have little impact on the eastward topographic tilt. On the other hand, the role of active tectonic deformations in the development of this topographic tilt remains uncertain for several reasons. First, the level of background seismic activity in the region is relatively low, with large-magnitude earthquakes ($Mb \geq 6$) being infrequent (Gangrade & Arora, 2000; Jaiswal & Sinha, 2007; Maurya et al., 2016; Saha et al., 2020). Moreover, seismic events tend to localize in the Proterozoic mobile belts, which are obliquely oriented relative to the tilt axis (Copley et al., 2014; Valdiya, 2001; Veeraswamy & Raval, 2005; Widdowson & Mitchell, 1999). Focal mechanisms along the western seaboard typically exhibit extensional characteristics, while those along the continental interior and eastern seaboard suggest strike-slip dynamics (Müller et al., 2015; Yamato et al., 2013). Taken together, these various lines of evidence suggest that the origin of the eastward topographic tilt in peninsular India remains an unresolved question, especially in the perspective of a geodynamic issue.

This article embarks on this topographic problem of peninsular India in light of isostatic dynamics, integrating a detailed analysis of the E-W topographic profiles and those obtained from a geodynamic model of the Indian plate tectonic setting. It is demonstrated from model simulations that the contrasting physical properties of the oceanic lithospheres below the Bay of Bengal and the Arabian Sea on the eastern and the western flanks of peninsular India have modulated the eastward-sloping asymmetric topographic development in peninsular India. This topographic gradient has driven all the major peninsular rivers to drain across the entire continental craton and ultimately fall into the Bay of Bengal.

2 The Indian Peninsular Plateau

2.1 Tectonic Setting

The Indian plate forms a complex geological relationship with its neighbouring tectonic plates, each significantly influencing the topography of the Indian subcontinent. Its northern boundary with the Eurasian Plate is marked by the remarkable Himalayan Mountain range and the vast Tibetan Plateau, both of which have developed over the past 50 million years as a result of the India-Asia continental collision (Ding et al., 2022; Royden et al., 2008). Their current topography reflects the interplay of decreasing convergence rates and isostatic adjustments, continuously reshaping elevations over time (Maiti et al., 2021). In contrast, Peninsular India (PI), illustrated in Figure 2, represents a stable Precambrian craton characterized by minimal recent tectonic activity (Gerya, 2014). A significant portion of IP is dominated by the Deccan volcanic province (Ghosh et al., 2024; Mittal et al., 2021; Mittal & Richards, 2021), flanked by the prominent Western and Eastern Ghats (its geological constitution is elaborated in S1; Figure S1). The continental lithosphere of IP interfaces with oceanic plates of varying sea-floor ages (Figure 2). In the Arabian Sea, the Carlsberg Ridge marks a divergent plate boundary, with lithospheric ages progressively increasing away from it. Conversely, the oceanic lithosphere of the Bay of Bengal (BOB), situated to the east of PI, is considerably older (Age ~ 140 Ma) than that of the Arabian Sea (Age ~ 60 Ma) (Figure 2). The BOB lithosphere ultimately meets the Sunda Trench, where the Indian Plate subducts beneath the Sunda and Burma plates (Steckler et al., 2016). Geophysical data indicate substantial variations in lithospheric thickness across the Bay of Bengal, with central regions exhibiting a thinner lithosphere of approximately 50-60 km compared to other areas (Dubey & Tiwari, 2022; Rao et al., 2016; Saha et al., 2021). These variations may stem from ongoing rifting and subsidence, influenced by mantle upwelling (Roy & Chatterjee, 2015). At the north-eastern margin of the Bay of Bengal, the Indian Plate establishes a convergent boundary with the Burmese Plate, resulting in significant lithospheric deformation and high seismicity in the region (Steckler et al., 2016) (Figure 2).

The Eastern Continental Margin (ECM) of Peninsular India stretches approximately 2,600 km and is classified as a passive continental margin. Current tectonic models suggest that the ECM originated from a rifting event during the Late Jurassic to Early Cretaceous period, when India, Antarctica, and Australia separated from the Gondwanaland (details of the tectonic evolution provided in S2; Figure S2) (Ali & Aitchison, 2008; Chatterjee et al., 2013; Gibbons et al., 2012). This is evidenced by rift-related grabens and sags near the shelf and the offshore basins. The processes of continental breakup have left geological signatures, such as the truncation of the northwest-southeast trending Godavari and Mahanadi rift valleys against the ECM (Biswas, 2003; Mishra et al., 1989, 1999). The ECM predominantly features the Eastern Ghats Proterozoic mobile belt (EGMB) (supplementary section S1; Figure S1), approximately 1,500 km long, extending from India's eastern coast to the southern tip of IP (Chetty & Murthy, 1994; Mishra et al., 1999). The tectonics of the Gondwanaland breakup during the Mesozoic Era also led to the formation of several continental-scale intra-cratonic sedimentary basins, including the Krishna-Godavari and Mahanadi basins in IP (Chatterjee et al., 2013).

On the western side of IP, the Western Continental Margin (WCM) extends north-south for about 2,200 km and includes diverse geological formations, such as Precambrian granitic belts, Mesozoic sedimentary layers, the Deccan volcanic province, and Paleocene to Recent sediments (Crawford, 1969; Kale, 2002; Meert & Pandit, 2015; Subrahmanyam & Chand, 2006). This margin is crucial for understanding the geodynamic evolution of the Arabian Sea and is considered a passive continental margin that formed during the Gondwanaland breakup in the Cretaceous period, which separated the Indian subcontinent from Africa and Madagascar, subsequently leading to the opening of the Arabian Sea through the initiation of the Carlsberg Ridge (Chatterjee et al., 2013, 2017; Subrahmanyam & Chand, 2006) (Figure S2). The WCM displays geological evidence of extensional tectonics, including rifted and faulted blocks, indicative of lithospheric stretching during the early stages of continental breakup. This extensional tectonics has facilitated the accumulation of sediments, presently preserved at the continental margin (Kale, 2002; Subrahmanyam & Chand, 2006). Geological studies suggest that the Arabian Sea began to open in the Late Jurassic to Early Cretaceous period (around 150 Ma) due to rifting between the Indian and

African plates, followed by seafloor spreading in the oceanic lithosphere (Chatterjee et al., 2013; Gaina et al., 2015) (details of the tectonic evolution provided in S2; Figure S2). The lithosphere beneath Arabian sea gradually thins towards the mid-ocean ridge system, particularly at the Carlsberg Ridge, which is a part of the larger Indian Ocean Ridge system (Chatterjee et al., 2013; Gaina et al., 2015) (Figure S2). The geological evolution of the Arabian Sea is further complicated by the interaction between the Indian Plate and the Eurasian Plate, which has facilitated ridge-push forces from the Carlsberg Ridge.

The geological setting of the WCM has been significantly influenced by the Deccan Traps, formed during the late Cretaceous period, around 66 Ma ago. The extensive outpouring of flood basalts associated with the breakup of the Indian plate from the African plate is linked to the Réunion hotspot beneath the Indian lithosphere (see supplementary section S2 for detail; Figure S2) (Chatterjee et al., 2013). Geomorphologically, the Deccan Traps exhibit a step-like topography characterized by thick basaltic lava flows covering over 500,000 square kilometers in west-central India. Some studies suggest that the underlying domal structure, resulting from the interaction of the Réunion plume with the lithosphere, has shaped the current plateau's topography (Cox, 1989; Radhakrishna, 1993). The WCM features the Western Ghats, a prominent mountain range along India's western coast. The formation of the Western Ghats is closely associated with the development of the western continental margin due to India's separation from Madagascar at around 90 Ma (Chatterjee et al., 2013, 2017). Its tectonic studies indicate that the range itself represents a fault escarpment formed by uplift and erosion rather than tectonic folding or orogeny (Chatterjee et al., 2013). The timing of uplift in the Western Ghats remains debated, with estimates ranging from the Late Cretaceous to the Early Cenozoic; this uplift is thought to have been influenced by both the thermal effects of Deccan volcanism and tectonic forces related to the rifting of the Indian plate (Cochran, 1983; Cox, 1980; Devey & Lightfoot, 1986; Gunnell et al., 2003; Gunnell & Fleitout, 1998; McKenzie, 1978; Roger Buck, 1986; Tiwari et al., 2006; Weissel & Karner, 1989; Widdowson & Cox, 1996). Geophysical studies suggest that the lithospheric thickness beneath the Western Ghats is relatively high, ranging from 100-120 km, indicating a stable cratonic region that has experienced minimal lithospheric thinning (Dubey & Tiwari, 2018; Gupta et al., 2018; Radha Krishna et al., 2002; Tiwari et al., 2006). Structurally, the Western Ghats exhibit a variety of geological features, including rifted margins, escarpments, and deeply incised valleys. The region's high topographic relief is generally attributed to a combination of tectonic uplift and differential erosion over millions of years (Mandal et al., 2015; Mandal et al., 2015).

2.2 Drainage Patterns

We studied the large-scale drainage patterns in peninsular India as they directly respond to the first-order topographic slopes in the continental region. All the major rivers show a common characteristic feature; they originate at the plateau's extreme western edge, a few kilometers away from the Arabian Sea coast and drain through the entire transect of peninsular plateau to finally fall into the Bay of Bengal (BOB) on the East. For example, the Godavari, Krishna, and Kaveri, which are the three longest rivers in this region, find their sources at the crest line in the Western Ghats and subsequently flow eastward to meet the BOB by cutting the Eastern Ghats Mountain barriers (Figure 1). Their east-directed courses clearly indicate an overall eastward tilt of the peninsular plateau.

The East coast of peninsular India stretches for about 2600 km, starting from the Sundarbans and ending at Kanyakumari (Figure 1; Figure 2), intervened by various physiographic features, such as river delta systems, vast coastal plains and extensively sediment deposits. The river systems in peninsular India are divided by the westward-flowing Narmada River. On the north of this river, the Ganga and associated rivers constitute the river system that collectively drains to south-west and then takes a sharp turn to south, eventually to fall into the BOB, forming the Sundarbans Delta, the largest delta in the world (Rogers & Goodbred, 2014). On south of the Narmada River, the peninsular plateau is drained by four major rivers: Mahanadi, Godavari, Krishna and Cauvery and associated minor rivers, e.g., Pennar and Palar and Thamirabarani and Vaigai; all of them flow into the BOB, producing isolated deltaic platforms at their mouths on the East coast (Figure 1).

The western coast of the Indian Peninsula broadly follows the Western Ghat Escarpments (WGE), a spectacular orographic feature that constitutes a linear relief at the western edge of the peninsular plateau, stretching for about 1600 km from the Tapi valley on north of Mumbai to the southern tip at Kanyakumari. All the major peninsular rivers discussed above originate from the WGE relief, on average, of 1200 m, and flow eastward over the plateau with elevations of more than 800 m. The escarpment shows west-directed embayment lines, formed due to intense erosion by westerly-flowing streams. The WGE serves as a N-S divide between eastward-flowing river systems (e.g., Godavari, Krishna and Cauvery) (Figure 1) and the westward-flowing short-range streams. Due to the lacks of rivers in the Arabian sea, the sedimentary thickness in the Arabian Sea is substantially thinner than that of the BOB.

2.3 Topographic Analysis

Using digital elevation maps (DEM) we prepared a series of E-W topographic profiles (Figure 3a-3b), covering the entire E-W stretch from the WGE crest line to the eastern flank of the Eastern Ghat Mountain ranges. The profiles were taken at a close interval (~ 180-200 km) to cover a N-S horizontal distance of 350-1200 km, as illustrated in Figure 3a-3b. They reveal topographic undulations in multiple wavelengths, which evidently reflect involvement of multiple factors, such as tectonic uplift, surface erosion, and rock types, in shaping the surface topography. In this study, we focus on the long-wavelength (first-order) topography (red colour in Figure 3a), considering it as a direct proxy of the lithospheric scale dynamics (Beaumont et al., 2001; Clark & Royden, 2000; Copley et al., 2011; Copley & Mckenzie, 2007; Maiti et al., 2021; Mandal et al., 2015; Neuharth et al., 2022; Neuharth et al., 2022; Pons et al., 2022). The first-order topography at any E-W transect in the peninsular plateau forms a recognizable eastward slope, with its elevations declining from ~800 meters on the WGE crest to ~200 meter at the extreme eastern edge (Figure 3a). The serial topographic profiles reveal a consistent change in the maximum WGE elevations from north to south, varying from ~380 meter and to ~950 meter (Figure 3a). On the eastern flank of the plateau the maximum elevation fluctuates between ~198 meter and ~390 meter (Figure 3a).

The peninsular plateau shows internal topographic heterogeneities on relatively smaller wavelengths, as elucidated in Figure 3a, where the surface topography forms a few elevation spikes in its central region, which die out in both the west and east directions. In contrast, the eastern flank of the plateau has markedly a gentler gradient. It is important to note that the plateau topography varies significantly from north to south, both along the Western and Eastern Ghat Mountain ranges. In the Western Ghats, the average elevation ranges from approximately 500 to 600 meters, while in the Eastern Ghats region, it averages around 375 meters, as depicted in Figure 3a. The topographic profile exhibits a sharp increase in elevation with steep slopes (average ~75°) along the western side of the WGE mountain range, followed by gentle slopes (average ~25°) on its eastern flank (Figure 4). The maximum elevation in the Western Ghats region reaches approximately 800 meters, whereas in the eastern part, it lies at around 650 meters (Figure 4). The height, however, increases sharply to form a narrow, about 100 km wide peak in the Eastern Ghats region (Figure 3a).

To evaluate the eastward tilt in the plateau, we calculated the overall first-order topographic slopes from each E-W section (procedures provided in Supplementary section S3), which are found to range from 0.008° to 0.3° (Figure 3a-3c). In the northern sector the plateau forms a topographic slope of ~ 0.008°- 0.006° (see Figure 3a) towards the BOB. The slope increases to 0.03° - 0.05° in the central sector of the peninsula. The southern part of the peninsula yields locally an eastward topographic slope of 0.1° (Figure 3a). To generalize the estimates of first-order topographic slopes, we performed a histogram analysis of the slope data. The most dominant topographic slope is found to be 0.05° in the far north and the central region of the Peninsula, which increases to ~ 0.1°-0.3° in the south (Figure 3c). Our comprehensive topographic slope analysis clearly suggests that the Indian Peninsular plateau maintains an overall eastward slope in the entire transect from north to south.

3 Geodynamic modelling

3.1 Approach

We implement numerical simulations based on a finite element method (FEM) approach to model the topographic evolution of the Indian Peninsula (IP), including the oceanic lithospheres beneath the Bay of Bengal (BOB) to the east and the Arabian Sea (AS) to the west of the IP (Figure 2). As discussed previously (section 2.1), the Arabian oceanic lithosphere is modeled with an age of 60 million years at the western IP passive margin, with its density varying as a function of lithospheric temperature. The BOB lithosphere, on the other hand, is assigned an average age of 140 million years, and its density is modeled with a constant average value of 3460 kg/m³ (see supplementary section in Afonso et al., 2007; Dasgupta et al., 2021), given the absence of an active ridge or significant variation in lithospheric age in this region. The initial model setup and boundary conditions are illustrated in Figure 5. To capture topographic variations in the IP in the north-south direction, we use a series of east-west cross-sections across the IP (Figure 6). For a detailed analysis, we focus on three specific sections: AB (IP length = 900 km), CD (IP length = 750 km), and EF (IP length = 600 km), which represent the northern, central, and southern segments of the IP, respectively (Figure 6). The E-W lithospheric stretches of the BOB and AS are also varied in the models accordingly, while maintaining a constant model domain length.

We model mantle rheology using a composite creep law that combines diffusion (η_{diff}) and dislocation (η_{disl}) creep processes. The creep laws for mantle silicates are described by an Arrhenius function for temperature and pressure dependence of the activation volume (V) and activation energy (E) (Hirth & Kohlstedt, 2003). The resulting diffusion- and dislocation-controlled viscosity is expressed as:

$$\eta_{diff/disl} = A^{\frac{-1}{n}} \dot{\varepsilon}^{\frac{1-n}{n}} exp\left(\frac{E+PV}{nRT}\right), \tag{1}$$

where A is a pre-factor, n is the stress exponent (n = 1 and 3.5 for diffusional and dislocation creep, respectively), R is the gas constant and P is the lithostatic pressure. A harmonic mean of the two types of viscosity is considered to find an effective model viscosity (η_{eff}),

$$\frac{1}{\eta_{eff}} = \frac{1}{\eta_{diff}} + \frac{1}{\eta_{disl}}. \tag{2}$$

The activation volumes (V) and activation energies (E) used in our modelling (details in Table 1) are consistent with experimental estimates for dry olivine (Karato & Wu, 1993). The pre-factor A for the upper mantle is chosen to satisfy two key observations: 1) an effective viscosity of approximately 10^{20} Pa s in the shallow part of the upper mantle (Hager, 1991), and 2) seismic anisotropy, which suggests that dislocation creep dominates in the upper mantle (Thorsten W. Becker, 2017). In our model, the top crustal layer is assigned a constant viscosity of 1×10^{26} Pa s. The strength of the mantle lithosphere is determined by the upper viscosity cut-off value (1×10^{26} Pa s) (Gerya et al., 2008). We model the crust and lithosphere as single, uniform layers without internal rheological stratification.

We numerically simulate the isostatic dynamics of IP in a time-evolving, dynamically consistent thermomechanical model. The model is developed in 2-D Cartesian domains within a theoretical framework of computational fluid dynamics (CFD) using the *Underworld2* code (Beucher et al., 2019; Cooper et al., 2017; Mansour et al., 2020; Sandiford et al., 2019; Sandiford & Moresi, 2019). This CFD simulation study assumes an incompressible Boussinesq fluid flow at low Reynolds Number, approximating the million-year scale kinematic state of Earth's mantle (Roy et al., 2024). We use two governing equations: the continuity equation and the momentum conservation equation to describe the spontaneous flows in the model. Their respective expressions are as follows:

$$\frac{\partial v_i}{\partial x_j} = 0 \tag{3}$$

$$-\frac{\partial P}{\partial x_i} + \frac{\partial \sigma_{ij}}{\partial x_j} + \rho g = 0, \tag{4}$$

where v_i is the velocity vector. In equation (4) inertial forces are negligible, as applicable to long term flows in the mantle. Applying the model boundary conditions (Figure 5), we numerically solve equations, (3) and (4) to find the velocity and pressure in the model domain, as described in the preceding paragraph. The thermal evolution in the geodynamic model is determined by combining advective heat transfer, thermal diffusion, and heat sources/sinks in the system.

Applying Boussinesq approximation, the model uses the following heat equation:

$$\frac{\partial T}{\partial t} + \boldsymbol{v}.\nabla T' = \kappa \nabla^2 T' + \frac{Q}{C_p}, \tag{5}$$

where $\kappa = \frac{k}{\rho C_p}$, which represents the thermal diffusivity. T' is replaced by the adiabatic temperature (T) of the system as a function of depth (z) obtained from the relation:

$$T = T' + z\left(\frac{\partial T}{\partial z}\right) = T' + z\left(\frac{\alpha g T_p}{C_p}\right), \tag{6}$$

where T_p is the mantle potential temperature and α is the coefficient of thermal expansion, which was set at a value of 3×10^{-5} K^{-1} (Roy et al., 2024). Considering C_p = 1260 J/kg/K for Earth's mantle (Roy et al., 2024), a resultant adiabatic temperature gradient of 0.4 K/km is added to the nonadiabatic mantle temperature. We impose constant (Dirichlet) and zero-flux (Neumann) temperature conditions on the top and bottom model boundaries, respectively to solve the energy equation. The initial model surface and bottom temperatures are set at 0°C and 1300°C, respectively.

To solve the governing equations, we meshed the 2D FEM domain (3000 km × 660 km) by smaller quadrilateral elements with a mesh resolution of 320 elements in the vertical direction, which provides an element width of ~2 km, and a particle density of 50 tracers per element (Sandiford & Moresi, 2019). We add passive tracers (P_1, P_2, P_3, P_4, & P_5) in the compositional field to track the plate motion and deformation in the model simulations at five different locations in the numerical models (Figure 5).

3.2 Model Results

3.2.1 The IP topography: a model analysis

The FE model simulations show an asymmetric topographic evolution in peninsular India, forming consistently eastward surface slopes on E-W transects from north to south. In the following descriptions we consider specifically three IP transects: (i) AB, (ii) CD and (iii) EF

(Figure 6) to elaborate the asymmetric topographic elements in the northern, central and southern segments of the continental mass.

The numerical model, representing the northern segment of the Indian Peninsula (NIP), consists of a continental lithospheric block (AB) with a horizontal extent of 900 km and a vertical thickness of 120 km (Figure 7a). At time t = 0, the model shows a uniform horizontal topography with no distinct surface slope (θ = 0°) (Figure 7b). As the simulation progresses to 0.1 Ma, the NIP lithospheric complex begins to dynamically adjust, producing an asymmetric first-order topography with an overall eastward slope of approximately 0.2°. By t = 0.21 Ma, the model surface in the continental region undergoes significant vertical uplift, as evidenced by the increasing elevations of passive markers (P2, P3, and P4) (Figure 7b). At P1 (western side), the NIP topography attains a height of approximately 5.65 km, which increases to a maximum of 6.29 km at P2 (eastern side). However, at P4 and P5, the maximum elevations are ~3.87 km and 0.55 km, respectively (Figure 7b). This east–west variation in elevation results in a first-order eastward topographic slope of 0.33°, which is notably steeper than the topographic gradients observed in the corresponding digital elevation map of peninsular India (discussed further in supplementary section S4). At t = 0.54 Ma, the topography of the NIP region continues to rise, with elevations of 8.47 km, 7.96 km, and 5.59 km at P2, P3, and P4, respectively. During this period, the eastward topographic slope steepens further to 0.37°.

The representative model for the Central Indian Peninsula (CIP) segment consists of a 120 km thick continental lithospheric block (CD) that extends 750 km in length (Figure 8a). This block is situated between two oceanic lithospheres, corresponding to the Bay of Bengal and the Arabian Sea. At the initial simulation time (t = 0 Ma), the model maintains a uniform, horizontal surface topography with a slope of θ = 0° (Figure 8b). As the simulation progresses, the CIP lithospheric block begins to dynamically adjust, forming asymmetric topography with a consistent eastward slope (Figure 8b), analogous to the trends observed in the NIP model. By t = 0.11 Ma, the CIP topography shows substantial elevation changes, as indicated by the positions of passive markers P2, P3, and P4 on the initial surface. At P2, the elevation (h) reaches a maximum of approximately 3.93 km, after which it decreases eastward to 3.34 km at P3. The elevation continues to decline further east after crossing a high of 2.34 km at P4 (Figure 8b). This lateral variation in elevation results in an eastward topographic slope of θ = 0.29°, which is consistent with observed natural landscape profiles

(Figure 8b and Figure 3c). By t = 0.63 Ma, the surface topography of the CIP continues to rise, with elevations at passive markers P2 (h = 8.31 km), P3 (h = 7.6 km), and P4 (h = 5.61 km) showing significant increases. At this stage of the simulation, the calculated θ increases to 0.51° and maintains an eastward trend across the CIP (Figure 8b).

The representative numerical model of the Southern India Peninsular (SIP) topography consists of a 120 km thick and 600 km long continental lithospheric block (EF), sandwiched between two oceanic lithospheres of contrasting ages: 40 Ma and 140 Ma in the Arabian Sea and the BOB east, respectively (Figure 9a). The simulation run at t = 0 Ma shows flat topography with horizontal surface ($\theta = 0^{\circ}$) (Figure 9b), which on dynamic adjustments evolves to an asymmetrically elevated topography at t = 0.11 Ma. To describe the topographic evolution, we choose three passive markers (P_2, P_3, P_4) on the surface of the initial model (Figure 9b). On the western side (P_1) the SIP gains a maximum height (h) of about 4.27 km, which continuously decreases to attain an elevation, $h = 3.12\ km$ at P_3, and ultimately decreases to a height of about $h = 2.02\ km$ at P_4. The differential elevation changes give rise to asymmetric surface topography that consistently slopes ($\theta = 0.32^{\circ}$) towards east (Figure 9b). A steep rise of topographic elevations occurs on the western side of the SIP section to produce a strong asymmetry of the surface topography with a large eastward slope ($\theta = 0.48^{\circ}$) at t = 0.22 Ma (Figure 9b) which further increases to $\theta = 0.58^{\circ}$ at t = 0.69 Ma.

3.2.2 Mantle flow patterns and surface dynamics

The BOB lithospheric subsidence sets in large-scale, westward sublithospheric mantle flows, which play the most crucial role in controlling the geodynamics of IP topography (Figure 10a, 10b, and 10c). The flows originate from a sublithospheric region beneath the central part of the BOB and follow curvilinear paths with predominantly horizontal velocity components. They eventually upwell at the western margin of IP. The west-ward flow is complemented by east-directed sub-lithospheric flows beneath the Arabian Sea, but significantly weaker than the westward counterparts. The two oppositely-directed mantle flows converge to form a focused upwelling zone beneath the western IP margin (Figure 10a, 10b, and 10c).

The velocity fields exhibit a striking contrast in the mantle regions beneath the eastern and western flanks of the IP lithosphere. In the eastern flank, a highly subdued flow regime develops, characterized by a stagnation zone within the lithosphere (Figure 10a, 10b, and

10c), indicating that the eastern IP lithosphere behaves as a relatively stable region. For instance, the sublithospheric velocity field in the NIP model (AB-section) shows strong horizontal flows (U_H = 3.23 cm/yr), with much smaller vertical components (U_V = 1.37 cm/yr) (Figure 9a). In contrast, the velocity field at the western margin is dominated by large vertical velocity components (U_V = 2.61 cm/yr). This westward gradient in vertical velocity (U_V) induces a rotational motion of the IP lithosphere, leading to the eastward tilting of the IP plateau. These velocity field patterns suggest that the eastward topographic tilt is primarily driven by upwelling mantle dynamics, localized at the western flank of the IP lithosphere.

Serial model simulations reveal a systematic variation in sublithospheric mantle flow patterns from the northern to the southern transects of the IP (Figure 10a, 10b, and 10c). As the E-W continental width of the IP decreases southward, the west-directed mantle flows extend beyond the western IP margin, encountering the weaker east-directed sublithospheric flows beneath the Arabian Sea. This interaction forms an upwelling zone at the ocean-continent boundary, resulting in the highest uplift velocities (U_V = 3.93 cm/yr) along the western margin of the IP (Fig 10c). Moving south, the location of this upwelling zone shifts eastward (Fig 10c), strengthening the upwelling dynamics and amplifying the rotational motion of the IP lithosphere. This shift is reflected in larger tilts of the topographic plateau in the southern sector of the IP (Fig 10c).

3.2.3 Synthesis of model and observed IP topography

The topographic analysis of the E-W serial sections clearly suggests a steady increase in topographic asymmetry from the northern to the southern regions of IP, reflecting a notable enhancement in the eastward slopes moving towards south. For Example, our NIP model (AB section) estimates that the northern peninsular region develops an eastward topographic slope ($\theta = 0.37^{\circ}$), which multiplies to attain a substantially larger value ($\theta = 0.58^{\circ}$) in the EF section considered in our SIP model. This striking increase in the first-order topographic slope of peninsular India is a convincing indication of the geodynamic forces driving this asymmetry becoming stronger at the southern region of IP, which is evident from the sub-lithospheric mantle flow pattern described in the preceding section. The model simulations show that the initial E-W horizontal extent of the Indian continent lithosphere (L) determines the upwelling location of westward sublithospheric mantle flows (Figure 10). Southwardly reducing θ allows the westward mantle flows to dominate over the eastward flow and upwells right at the ocean-continent lithospheric boundary. The upwelling thereby exerts vertical forces on the entire IP lithospheric stretch to the west, setting a favourable mechanical condition to facilitate the lithospheric rotation.

4 Discussion

4.1 Dynamics of the Indian Peninsular River System

The model simulations (Section 3.2) suggest that the persistently eastward flows of the Indian peninsular rivers over vast distances (hundreds of kilometres) are primarily driven by the continental scale (first-order) topographic gradient, which originates from a complex geodynamic influence of the sub-lithospheric mantle flows, as discussed in section 3.2.2. The resulting escarpment relief acts as a barrier, preventing from eroding the terrain along shorter, westward pathways toward the Arabian Sea. The resilience of the WG escarpment against the erosion at high rates (mean erosion rate: 48.6 ± 20.9 mMa^{-1}, Mandal et al., 2015; Mandal et al., 2015) underscores a dynamic interplay between tectonics and fluvial processes to sustain its positive physiographic relief on long time scales. The ongoing tectonic uplift (Figure 10) of the escarpment counters erosion-driven denudation, maintaining the eastward topographic slope and guiding the river systems toward the Bay of Bengal. This eastward polarization of the drainage pattern has led to a geomorphic asymmetry in the IP landform over geological time (Figure 1).

The major rivers originating from the Deccan Plateau, such as the Godavari, Krishna, and Cauvery, have transported vast quantities of sediment, depositing them into the Bay of Bengal over an extended geological timeframe, suggesting that the river system has been consistently transporting continental sediments to the Bay of Bengal for a significant period (Rao et al., 1997). This continuous sediment supply implies a remarkably stable and persistent eastward drainage pattern, which is a direct consequence of long-term tectonic activity across the Indian Plate (IP). Moreover, the sedimentary records preserved in the Bay of Bengal offer a valuable archive of the region’s tectonic and climatic history. The ongoing deposition of sediments reflects a dynamic landscape where the stability of the eastward-sloping topography has been maintained over millions of years. These long-term sedimentation patterns point to sustained tectonic activity in the Indian craton, which has played a crucial role in preserving the eastward-flowing drainage system. Our numerical model results (Figures 7, 8 and 9) further support the idea that the long-term eastward topographic gradient has been a key feature of the landscape’s evolution in peninsular India.

4.2 Asymmetric PI topography and tectonic models

The Indian craton is positioned between two oceanic lithospheres of contrasting ages: the relatively young Indian Ocean lithosphere to the west and the older Bay of Bengal lithosphere to the east. The Indian lithosphere, which is part of the larger Indo-Australian Plate has been engaged in complex interactions with the surrounding plates. Historically, the Indian plate has undergone a large northward drift, primarily driven by mantle convection and plate tectonic forces, following its breakup from the ancient supercontinent Gondwana. This drift ultimately led to the collision with the Eurasian plate, giving rise to the Himalayan orogeny. However, this northward movement alone cannot explain the persistent eastward tilt of the peninsular topography. The sharply elevated, linear, north-south trending topographic high, most notably represented by the Western Ghats escarpment, suggests focused tectonic activity along the western margin. This is further evidenced by observable seismic activity in the region (Catherine et al., 2007; Jha et al., 2023; Sribin et al., 2024). These observations point to the necessity for alternative tectonic models that can better account for the current movements and topographic features of the Indian plate.

A plume model has been proposed to explain the development of peninsular topography, suggesting that mantle plumes are responsible for the uplift and volcanic activity observed in the region (Cox, 1980, 1989; Watts & Cox, 1989; Widdowson & Cox, 1996). However, this model fails to fully explain the linear topography, which several workers have shown to be a product of neotectonic movements (Mandal et al., 2017; Mandal et al., 2015; Mandal et al., 2015). In addition, plume-driven topography is typically axisymmetric, which contrasts sharply with the N-S trending linear elevations of the Western Ghats with east-directed topographic slopes, the magnitudes of which increases from north to south, as shown in Figure 3. Furthermore, paleo-topographic studies indicate that the plume event that occurred around 65 Ma ago cannot sustain the extremely steep topographic slopes observed in the Western Ghats over such a long geological timescale. The persistence of these slopes suggests that the Western Ghats must have undergone slow, continuous uplift in more recent geological times (Richards et al., 2016). The ongoing uplift history is not in agreement with the rapid, short-lived topographic changes typically associated with mantle plume events. In summary, the plume model does not seem to adequately account for the long-term topographic stability and eastward tilting observed in the Indian peninsula. A geodynamic model used to examine the asymmetric IP topography must be in compliance with the contrasting subsidence rates between the Bay of Bengal (model subsidence rate = 1.67 cm/year) and the Arabian Sea (Figure 11a) and the ongoing tectonic uplift of the Western Ghats. Our study reveals a connection between this differential subsidence with the uplift tectonics of the WG in controlling the asymmetric IP topography, and maintaining spatially persistent eastward slopes.

4.3 The Western Ghat Escarpment: A Geodynamic Response

The Western Ghats (WG) escarpment exhibits a step-like form, characterized by a dramatic elevation drop from approximately 2,000 m to 500 m towards the west. Several hypotheses have been proposed to explain the origin of this escarpment, though each has its own limitations. One hypothesis suggests that the escarpment formed as a rift shoulder during the break-up of Gondwana, following the separation of the Indian plate from Madagascar and Africa (Chatterjee et al., 2013). However, this model does not fully account for the continuous uplift observed in more recent geological times (Radhakrishna, 1993; Richards et al., 2016). Another hypothesis proposes that the escarpment resulted from flexural uplift due to the loading and unloading of sediments along the western margin. While this explanation can account for some aspects of the topography, it fails to explain the linearity of the escarpment and the specific north-south topographic variation observed in the Western Ghats. A third hypothesis attributes the formation of the escarpment to mantle plume activity, suggesting that thermal buoyancy could have uplifted the region. However, plume-driven topography is typically axisymmetric, whereas the Western Ghats form a long, linear feature, which does not align with this model as discussed in the preceding section.

The shortcomings discussed above highlight the need for a more comprehensive model that offers a self-consistent interpretation of the Western Ghats (WG) dynamics, based on observed geological and geophysical signatures. These include neotectonic movements (Mandal et al., 2017), the maintenance of anomalously steep topography despite surface erosion(Mandal et al., 2015), seismic activity (Jha et al., 2023), and E-W seismic anisotropy in the sublithospheric mantle (Jaiswal & Sinha, 2007). Collectively, these geological signals suggest that the origin of the Western Ghats is linked to deep-lithospheric processes. Our geodynamic modelling demonstrates that the Indian plate's tectonic setting, with contrasting lithospheric ages of the Bay of Bengal (BOB) and the Arabian Sea, generates E- and W-directed mantle flows, respectively. These flows converge into a focused upwelling zone at the western margin of the Indian craton, leading to the uplift of the Western Ghats and the formation of a topographic high. The presence of E-W seismic anisotropy (Becker et al., 2012), (Figure 11b) observed in the region, provides strong evidence supporting westward sublithospheric mantle flows in our model. Furthermore, this geodynamic framework explains the ongoing uplift of the Western Ghats, which is necessary to sustain the steep slopes of the WG Escarpment over geological timescales. In conclusion, the dynamic topography of the Western Ghats is primarily a result of lithosphere-mantle kinematic interactions, driven by westward sublithospheric mantle flows beneath the Bay of Bengal region (Figure 12).

The Bay of Bengal, with its denser lithosphere, has experienced significantly higher subsidence compared to its counterpart, the Arabian Sea, to the west (Figure 11a) This differential subsidence has led to focused uplift along the western margin of the Indian Peninsula (IP), as demonstrated in the model simulations presented in Section 3.2. Our geodynamic model suggests that the uplift rate in the Western Ghats has been primarily influenced by the higher subsidence rates in the Bay of Bengal, a correlation supported by observed subsidence rates in the Bay and the uplift rates in the Western Ghats. The numerical simulations are consistent with these observed rates, providing robust validation for our model results. The differential subsidence in the oceanic basins on either side of the IP (*cf.* Figure 11a), combined with deep-mantle flow dynamics, is the primary cause of the topographic asymmetry, which is reflected in the consistent eastward surface slopes and drainage patterns. This model not only explains the present-day topography of the Western Ghats but also offers a framework for understanding the long-term evolution of the IP's topography on a continental scale (Figure 12).

4.4 The Eastward Topographic Slopes: Model Estimates

The model results suggest that the southward increase in topographic slope is a consequence of the westward migration of the mantle upwelling zone. This migration becomes an effective factor in rotating the continental lithosphere of narrower width and developing steeper surface slopes in the south. Our model estimates qualitatively align with the observed north-to-south variation in topographic slopes discussed above. Despite the overall success of the model in capturing the qualitative trends in topographic slopes, the estimated values, however, tend to overestimate the actual slope magnitudes as measured from the Digital Elevation Model (DEM). Such discrepancies are common in geodynamic modeling, where simplifications and assumptions that are often necessary to address the complexities of natural systems can result in some discrepancies (see Supplementary section S4 for further discussions). In the case of the Western Ghats and the Indian Peninsular Plateau (IP), this overestimation is likely due to the exclusion of synkinematic surface erosion in the current model. It is well established that surface slopes evolve through the combined effects of tectonic uplift and concurrent erosion processes. Studies have shown quantitatively that erosion can significantly modify topographic slopes (e.g.,DiBiase & Whipple, 2011). In regions like the Western Ghats, where intense rainfall, tropical climates, and high erosion rates are prevalent, the topographic slopes are significantly reduced by surface erosion, as weathering and fluvial processes dominate the landscape evolution (Mandal et al., 2015). The major rivers originating from the Western Ghats—such as the Godavari, Krishna, and Cauvery—transport vast quantities of sediment eastward, ultimately depositing them in the Bay of Bengal. These sediment accumulations provide clear evidence of the strong erosional forces shaping the topographic slopes of the region. Since the present model primarily focuses on tectonic uplift and mantle dynamics while excluding the influence of erosion, it tends to somewhat overestimate the magnitudes of the eastward slopes in the IP. Although the model overestimates the topographic slopes, it offers valuable insights into the underlying tectonic and mantle dynamics that have shaped the Indian Peninsular Plateau.

5 Conclusions

This study provides a novel geodynamic perspective on the first-order asymmetric topography of the Indian Peninsular Plateau, revealing its connection to the broader plate tectonic configuration. A key finding is that a significant lithospheric density difference between the Bay of Bengal and the Arabian Sea, due to their contrasting ages, plays a crucial role in generating gravitational dynamics that tilt the plateau to the east. This dynamic condition induces both westward and eastward sub-lithospheric mantle flows beneath the Bay of Bengal and the Arabian Sea. The westward mantle flow predominates, capturing nearly the entire sub-lithospheric region of the Indian continent before encountering the eastward flows, which leads to upwelling along the western margin of the Peninsular India (IP). This focused upwelling causes the tilt of the plateau, resulting in a first-order topographic slope to the east. The magnitude of this eastward slope increases progressively from the northern to the southern part of the Peninsular India. Model simulations indicate that this southward intensification of the topographic slope is the result of the westward migration of the upwelling zone. Along the western margin of the plateau, the Peninsular India features a prominent physiographic feature: the Western Ghats, a north-south trending escarpment that stretches for approximately 1300 kilometers and exhibits a significant relative relief of ~ 800 meters. This study suggests that the Western Ghats escarpment is a direct manifestation of large-scale geodynamic processes. The differential subsidence in the Bay of Bengal generates westward mantle flows, which focus into upwelling along the western edge of Peninsular India. This upwelling results in positive topographic relief, particularly along the western flank of the Peninsular Craton, leading to the formation of the Western Ghats escarpment. Finally, the geodynamic model presented here integrates the development of the tilted Peninsular Plateau with subsidence in the Bay of Bengal and focused uplift along the Western Ghats.

Acknowledgements

The DST-SERB has supported this work through the J. C. Bose fellowship (JBR/2022/000003) to NM. JS is supported by a senior research fellowship (SRF) from DST-INSPIRE (IF170697), India. JS is thankful to Soham Banerjee and Ayan Patsa for reading the earlier version of the manuscript.

Data Availability Statement

We use open-source code *Underworld2* (https://github.com/underworldcode/underworld2) (Beucher et al., 2019; Mansour et al., 2020) which is available online under the terms of General Public License (GNU). The model data files to reproduce the graph and the DEM topography can be accessed in Zenodo repository (https://doi.org/10.5281/zenodo.14416339) (Sen et al., 2024).

References

Afonso, J. C., Ranalli, G., & Fernàndez, M. (2007). Density structure and buoyancy of the oceanic lithosphere revisited. *Geophysical Research Letters*, *34*(10). https://doi.org/10.1029/2007GL029515

Ali, J. R., & Aitchison, J. C. (2008). Gondwana to Asia: Plate tectonics, paleogeography and the biological connectivity of the Indian sub-continent from the Middle Jurassic through latest Eocene (166–35 Ma). *Earth-Science Reviews*, *88*(3–4), 145–166. https://doi.org/10.1016/J.EARSCIREV.2008.01.007

Asish, L. C., Parvez, I. A., & Kühn, D. (2016). Probabilistic earthquake hazard assessment for Peninsular India. *Journal of Seismology*, *20*(2), 629–653. https://doi.org/10.1007/S10950-015-9548-2/METRICS

Beaumont, C., Jamieson, R. A., Nguyen, M. H., & Lee, B. (2001). Himalayan tectonics explained by extrusion of a low-viscosity crustal channel coupled to focused surface denudation. *Nature*, *414*(6865), 738–742. https://doi.org/10.1038/414738a

Becker, T. W., Lebedev, S., & Long, M. D. (2012). On the relationship between azimuthal anisotropy from shear wave splitting and surface wave tomography. *Journal of Geophysical Research: Solid Earth*, *117*(B1). https://doi.org/10.1029/2011JB008705

Becker, Thorsten W. (2017). Superweak asthenosphere in light of upper mantle seismic anisotropy. *Geochemistry, Geophysics, Geosystems*, *18*(5), 1986–2003. https://doi.org/10.1002/2017GC006886

Beucher, R., Moresi, L., Giordani, J., Mansour, J., Sandiford, D., Farrington, R., et al. (2019). UWGeodynamics: A teaching and research tool for numerical geodynamic modelling. *Journal of Open Source Software*, *4*(36), 1136. https://doi.org/10.21105/JOSS.01136

Bishop, P. (2007). Long-term landscape evolution: linking tectonics and surface processes. *Earth Surface Processes and Landforms*, *32*(3), 329–365. https://doi.org/10.1002/ESP.1493

Biswas, S. K. (2003). Regional tectonic framework of the Pranhita–Godavari basin, India. *Journal of Asian Earth Sciences*, *21*(6), 543–551. https://doi.org/10.1016/S1367-9120(02)00145-1

Bonnet, N. J., Beauvais, A., Arnaud, N., Chardon, D., & Jayananda, M. (2014). First 40Ar/39Ar dating of intense Late Palaeogene lateritic weathering in Peninsular India. *Earth and Planetary Science Letters*, *386*, 126–137. https://doi.org/10.1016/J.EPSL.2013.11.002

Bonnet, N. J., Beauvais, A., Arnaud, N., Chardon, D., & Jayananda, M. (2016). Cenozoic lateritic weathering and erosion history of Peninsular India from 40Ar/39Ar dating of supergene K–Mn oxides. *Chemical Geology*, *446*, 33–53. https://doi.org/10.1016/J.CHEMGEO.2016.04.018

Campanile, D., Nambiar, C. G., Bishop, P., Widdowson, M., & Brown, R. (2008a). Sedimentation record in the Konkan-Kerala Basin: Implications for the evolution of the Western Ghats and the Western Indian passive margin. *Basin Research*, *20*(1), 3–22. https://doi.org/10.1111/J.1365-2117.2007.00341.X/CITE/REFWORKS

Campanile, D., Nambiar, C. G., Bishop, P., Widdowson, M., & Brown, R. (2008b). Sedimentation record in the Konkan–Kerala Basin: implications for the evolution of the Western Ghats and the Western Indian passive margin. *Basin Research*, *20*(1), 3–22. https://doi.org/10.1111/J.1365-2117.2007.00341.X

Catherine, J. K., Gahalaut, K., & Gahalaut, V. K. (2007). Role of flexure in earthquake triggering along the Western Ghat escarpment, India. *Journal of Asian Earth Sciences*, *31*(2), 104–111. https://doi.org/10.1016/J.JSEAES.2007.04.005

Chandra, U. (1977). Earthquakes of peninsular India—a seismotectonic study. *Bulletin of the Seismological Society of America*, *67*(5), 1387–1413. https://doi.org/10.1785/BSSA0670051387

Chatterjee, S., Goswami, A., & Scotese, C. R. (2013). The longest voyage: Tectonic, magmatic, and paleoclimatic evolution of the Indian plate during its northward flight from Gondwana to Asia. *Gondwana Research*, *23*(1), 238–267. https://doi.org/10.1016/J.GR.2012.07.001

Chatterjee, S., Scotese, C. R., & Bajpai, S. (2017). The Restless Indian Plate and Its Epic Voyage from Gondwana to Asia: Its Tectonic, Paleoclimatic, and Paleobiogeographic Evolution. *Geological Society of America*. https://doi.org/10.1130/2017.2529(A)

Chetty, T. R. K., & Murthy, D. S. N. (1994). Collision tectonics in the late Precambrian Eastern Ghats Mobile Belt: mesoscopic to satellite-scale structural observations. *Terra Nova*, *6*(1), 72–81. https://doi.org/10.1111/J.1365-3121.1994.TB00635.X

Clark, M. k, & Royden, L. H. (2000). Topographic ooze: Building the eastern margin of Tibet by lower crustal flow. *Geology*, *28(8)*(8), 703–706. https://doi.org/https://doi.org/10.1130/0091-7613(2000)28%3C703:TOBTEM%3E2.0.CO;2

Cochran, J. R. (1983). Effects of finite rifting times on the development of sedimentary basins. *Earth and Planetary Science Letters*, *66*(C), 289–302. https://doi.org/10.1016/0012-821X(83)90142-5

Collier, J. S., Sansom, V., Ishizuka, O., Taylor, R. N., Minshull, T. A., & Whitmarsh, R. B. (2008). Age of Seychelles–India break-up. *Earth and Planetary Science Letters*, *272*(1–2), 264–277. https://doi.org/10.1016/J.EPSL.2008.04.045

Cooper, C. M., Miller, M. S., & Moresi, L. (2017). The structural evolution of the deep continental lithosphere. *Tectonophysics*, *695*, 100–121. https://doi.org/10.1016/j.tecto.2016.12.004

Copley, A., & Mckenzie, D. (2007). Models of crustal flow in the India-Asia collision zone. *Geophysical Journal International*, *169*(2), 683–698. https://doi.org/10.1111/J.1365-246X.2007.03343.X/2/M_169-2-683-TBL001.JPEG

Copley, A., Avouac, J. P., & Wernicke, B. P. (2011). Evidence for mechanical coupling and strong Indian lower crust beneath southern Tibet. *Nature 2011 472:7341*, *472*(7341), 79–81. https://doi.org/10.1038/nature09926

Copley, A., Mitra, S., Sloan, R. A., Gaonkar, S., & Reynolds, K. (2014). Active faulting in apparently stable peninsular India: Rift inversion and a Holocene-age great earthquake on the Tapti Fault. *Journal of Geophysical Research: Solid Earth*, *119*(8), 6650–6666. https://doi.org/10.1002/2014JB011294

Cox, K. G. (1980). A Model for Flood Basalt Vulcanism. *Journal of Petrology*, *21*(4), 629–650. https://doi.org/10.1093/PETROLOGY/21.4.629

Cox, K. G. (1989). The role of mantle plumes in the development of continental drainage patterns. *Nature*, *342*(6252), 873–877. https://doi.org/10.1038/342873A0

Crawford, A. R. (1969). Reconnaissance Rb-Sr Dating of the Precambrian Rocks of Southern Peninsular India. *Journal of the Geological Society of India*, *10*(2), 117–166. https://doi.org/10.17491/JGSI/1969/100201

Dasgupta, R., Sen, J., & Mandal, N. (2021). Bending curvatures of subducting plates: old versus young slabs. *Geophysical Journal International*, *225*(3), 1963–1981. https://doi.org/10.1093/GJI/GGAB070

DeCelles, P. G., Quade, J., Kapp, P., Fan, M., Dettman, D. L., & Ding, L. (2007). High and dry in central Tibet during the Late Oligocene. *Earth and Planetary Science Letters*, *253*(3–4), 389–401. https://doi.org/10.1016/J.EPSL.2006.11.001

Devey, C. W., & Lightfoot, P. C. (1986). Volcanological and tectonic control of stratigraphy and structure in the western Deccan traps. *Bulletin of Volcanology*, *48*(4), 195–207. https://doi.org/10.1007/BF01087674/METRICS

DiBiase, R. A., & Whipple, K. X. (2011). The influence of erosion thresholds and runoff variability on the relationships among topography, climate, and erosion rate. *Journal of Geophysical Research: Earth Surface*, *116*(F4). https://doi.org/10.1029/2011JF002095

Ding, L., Kapp, P., Cai, F., Garzione, C. N., Xiong, Z., Wang, H., & Wang, C. (2022). Timing and mechanisms of Tibetan Plateau uplift. *Nature Reviews Earth & Environment 2022 3:10*, *3*(10), 652–667. https://doi.org/10.1038/s43017-022-00318-4

Dole, G., Das, S., & Kale, V. S. (2022). Tectonic framework of geomorphic evolution of the Deccan Volcanic Province, India. *Earth-Science Reviews*, *228*, 103988. https://doi.org/10.1016/J.EARSCIREV.2022.103988

Dubey, C. P., & Tiwari, V. M. (2018). Gravity Anomalies and Crustal Thickness Variations over the Western Ghats. *Journal of the Geological Society of India*, *92*(5), 517–522. https://doi.org/10.1007/S12594-018-1059-7/METRICS

Dubey, C. P., & Tiwari, V. M. (2022). Lithospheric-mantle modification beneath the thick sedimentary fan of Bay of Bengal: Inference from the 3D gravity model. *Tectonophysics*, *826*, 229253. https://doi.org/10.1016/J.TECTO.2022.229253

Ellis, M. A., Densmore, A. L., & Anderson, R. S. (1999). Development of mountainous topography in the Basin Ranges, USA. *Basin Research*, *11*(1), 21–41. https://doi.org/10.1046/J.1365-2117.1999.00087.X/CITE/REFWORKS

Fang, X., Dupont-Nivet, G., Wang, C., Song, C., Meng, Q., Zhang, W., et al. (2020). Revised chronology of central Tibet uplift (Lunpola Basin). *Science Advances*, *6*(50). https://doi.org/10.1126/SCIADV.ABA7298/SUPPL_FILE/ABA7298_SM.PDF

Gaina, C., Van Hinsbergen, D. J. J., & Spakman, W. (2015). Tectonic interactions between India and Arabia since the Jurassic reconstructed from marine geophysics, ophiolite geology, and seismic tomography. *Tectonics*, *34*(5), 875–906. https://doi.org/10.1002/2014TC003780

Gangrade, B. K., & Arora, S. K. (2000). Seismicity of the Indian peninsular shield from regional earthquake data. *Pure and Applied Geophysics*, *157*(10), 1683–1705. https://doi.org/10.1007/PL00001056/METRICS

Gerya, T. V., Perchuk, L. L., & Burg, J. P. (2008). Transient hot channels: Perpetrating and regurgitating ultrahigh-pressure, high-temperature crust–mantle associations in collision belts. *Lithos*, *103*(1–2), 236–256. https://doi.org/10.1016/J.LITHOS.2007.09.017

Gerya, Taras. (2014). Precambrian geodynamics: Concepts and models. *Gondwana Research*, *25*(2), 442–463. https://doi.org/10.1016/J.GR.2012.11.008

Ghosh, D., Sen, J., & Mandal, N. (2024). Periodicity in the Deccan Volcanism Modulated by Plume Perturbations at the Mid-Mantle Transition Zone. *Journal of Geophysical Research: Solid Earth*, *129*(6), e2024JB029020. https://doi.org/10.1029/2024JB029020

Gibbons, A. D., Barckhausen, U., Van Den Bogaard, P., Hoernle, K., Werner, R., Whittaker, J. M., & Müller, R. D. (2012). Constraining the Jurassic extent of Greater India: Tectonic evolution of the West Australian margin. *Geochemistry, Geophysics, Geosystems*, *13*(5). https://doi.org/10.1029/2011GC003919

Gunnell, Y., & Fleitout, L. (1998). Shoulder uplift of the Western Ghats passive margin, India: a denudational model. *Earth Surface Processes and Landforms*, *23*(5), 391–404. Retrieved from https://onlinelibrary.wiley.com/doi/abs/10.1002/(SICI)1096-9837(199805)23:5

Gunnell, Y., Gallagher, K., Carter, A., Widdowson, M., & Hurford, A. J. (2003). Denudation history of the continental margin of western peninsular India since the early Mesozoic – reconciling apatite fission-track data with geomorphology. *Earth and Planetary Science Letters*, *215*(1–2), 187–201. https://doi.org/10.1016/S0012-821X(03)00380-7

Gupta, S., Kanna, N., Kumar, S., & Sivaram, K. (2018). Crustal Thickness and Composition Variation along the Western Ghats of India through Teleseismic Receiver Function Analysis. *Journal of the Geological Society of India*, *92*(5), 523–528. https://doi.org/10.1007/S12594-018-1061-0/METRICS

Hager, B. H. (1991). Mantle Viscosity: A Comparison of Models from Postglacial Rebound and from the Geoid, Plate Driving Forces, and Advected Heat Flux. In *Glacial Isostasy, Sea-Level and Mantle Rheology* (pp. 493–513). Dordrecht: Springer Netherlands. https://doi.org/10.1007/978-94-011-3374-6_23

Heintz, M., Kumar, V. P., Gaur, V. K., Priestley, K., Rai, S. S., & Prakasam, K. S. (2009). Anisotropy of the Indian continental lithospheric mantle. *Geophysical Journal International*, *179*(3), 1341–1360. https://doi.org/10.1111/J.1365-246X.2009.04395.X/3/179-3-1341-FIG012.JPEG

Hirth, G., & Kohlstedt, D. (2003). Rheology of the upper mantle and the mantle wedge: a view from the experimentalists. *Geophysical Monograph-American Geophysical Union*, *138*, 83–106.

Hoggard, M. J., White, N., & Al-Attar, D. (2016). Global dynamic topography observations reveal limited influence of large-scale mantle flow. *Nature Geoscience 2016 9:6*, *9*(6), 456–463. https://doi.org/10.1038/ngeo2709

Houseman, G., & England, P. (1993). Crustal thickening versus lateral expulsion in the Indian-Asian continental collision. *Journal of Geophysical Research: Solid Earth*, *98*(B7), 12233–12249. https://doi.org/10.1029/93JB00443

Illa, B., Reshma, K. S., Kumar, P., Srinagesh, D., Haldar, C., Kumar, S., & Mandal, P. (2021). Pn tomography and anisotropic study of the Indian shield and the adjacent regions. *Tectonophysics*, *813*, 228932. https://doi.org/10.1016/J.TECTO.2021.228932

Jaiswal, K., & Sinha, R. (2007). Probabilistic Seismic-Hazard Estimation for Peninsular India. *Bulletin of the Seismological Society of America*, *97*(1B), 318–330. https://doi.org/10.1785/0120050127

Jha, K., Padma Rao, B., Sribin, C., & Silpa, S. (2023). Analysis of seismic noise of broadband seismological stations installed along the Western Ghats. *Journal of Seismology*, *27*(2), 325–342. https://doi.org/10.1007/S10950-023-10138-8/FIGURES/11

Kailasam, L. N. (1975). Epeirogenic studies in India with reference to recent vertical movements. *Tectonophysics*, *29*(1–4), 505–521. https://doi.org/10.1016/0040-1951(75)90178-X

Kale, V. S. (2002). Fluvial geomorphology of Indian rivers: an overview. *Progress in Physical Geography: Earth and Environment*, *26*(3), 400–433. https://doi.org/10.1191/0309133302PP343RA

Karato, S., & Wu, P. (1993). Rheology of the Upper Mantle: A Synthesis. *Science*, *260*(5109), 771–778. https://doi.org/10.1126/SCIENCE.260.5109.771

Kent, D. V., & Muttoni, G. (2008). Equatorial convergence of India and early Cenozoic climate trends. *Proceedings of the National Academy of Sciences of the United States of America*, *105*(42), 16065–16070. https://doi.org/10.1073/PNAS.0805382105/ASSET/C392017F-5074-45AD-A735-13E0D4AC2513/ASSETS/GRAPHIC/ZPQ9990849560003.JPEG

Kirby, E., & Whipple, K. X. (2012). Expression of active tectonics in erosional landscapes. *Journal of Structural Geology*, *44*, 54–75. https://doi.org/10.1016/J.JSG.2012.07.009

Kumar, V. P., Prakasam, K. S., Rai, S. S., & Gupta, S. (2015). Upper-mantle anisotropy beneath the south Indian Shield: Influenced by ancient and recent Earth processes. *Lithosphere*, *7*(2), 108–116. https://doi.org/10.1130/L405.1

Maiti, G., Roy, A., Sen, J., & Mandal, N. (2021). Impact of Decelerating India-Asia Convergence on the Crustal Flow Kinematics in Tibet: An Insight From Scaled Laboratory Modeling. *Geochemistry, Geophysics, Geosystems*, *22*(11), e2021GC009967. https://doi.org/10.1029/2021GC009967

Mandal, N., Bose, S., Baruah, A., & Sarkar, S. (2015). First-order topography of the Himalayan Mountain belt: A deep-crustal flow analysis. *Geological Society Special Publication*, *412*(1), 5–23. https://doi.org/10.1144/SP412.9/ASSET/AE19F504-089A-45E4-9C17-2024891F2E48/ASSETS/GRAPHIC/SP412-1190F11.JPEG

Mandal, P. (2011). Upper mantle seismic anisotropy in the intra-continental Kachchh rift zone, Gujarat, India. *Tectonophysics*, *509*(1–2), 81–92. https://doi.org/10.1016/J.TECTO.2011.05.013

Mandal, S. K., Fellin, M. G., Burg, J. P., & Maden, C. (2015). Phanerozoic surface history of southern Peninsular India from apatite (U-Th-Sm)/He data. *Geochemistry, Geophysics, Geosystems*, *16*(10), 3626–3648. https://doi.org/10.1002/2015GC005977

Mandal, S. K., Lupker, M., Burg, J. P., Valla, P. G., Haghipour, N., & Christl, M. (2015). Spatial variability of 10Be-derived erosion rates across the southern Peninsular Indian escarpment: A key to landscape evolution across passive margins. *Earth and Planetary Science Letters*, *425*, 154–167. https://doi.org/10.1016/J.EPSL.2015.05.050

Mandal, S. K., Burg, J. P., & Haghipour, N. (2017). Geomorphic fluvial markers reveal transient landscape evolution in tectonically quiescent southern Peninsular India. *Geological Journal*, *52*(4), 681–702. https://doi.org/10.1002/GJ.2833

Mansour, J., Giordani, J., Moresi, L., Beucher, R., Kaluza, O., Velic, M., et al. (2020). Underworld2: Python Geodynamics Modelling for Desktop, HPC and Cloud. *Journal of Open Source Software*, *5*(47), 1797. https://doi.org/10.21105/JOSS.01797

Maurya, S., Montagner, J. P., Kumar, M. R., Stutzmann, E., Kiselev, S., Burgos, G., et al. (2016). Imaging the lithospheric structure beneath the Indian continent. *Journal of Geophysical Research: Solid Earth*, *121*(10), 7450–7468. https://doi.org/10.1002/2016JB012948

McKenzie, D. (1978). Some remarks on the development of sedimentary basins. *Earth and Planetary Science Letters*, *40*(1), 25–32. https://doi.org/10.1016/0012-821X(78)90071-7

Meert, J. G., & Pandit, M. K. (2015). The archaean and proterozoic history of Peninsular India: Tectonic framework for precambrian sedimentary basins in India. *Geological Society Memoir*, *43*, 29–54. https://doi.org/10.1144/M43.3/ASSET/B95394B5-5AB9-4E56-8259-13D038FF2A4E/ASSETS/IMAGES/LARGE/M43_CH03F13.JPG

Minár, J., Evans, I. S., & Jenčo, M. (2020). A comprehensive system of definitions of land surface (topographic) curvatures, with implications for their application in geoscience modelling and prediction. *Earth-Science Reviews*, *211*, 103414. https://doi.org/10.1016/J.EARSCIREV.2020.103414

Mishra, D. C., Gupta, S. B., & Venkatarayudu, M. (1989). Godavari rift and its extension towards the east coast of India. *Earth and Planetary Science Letters*, *94*(3–4), 344–352. https://doi.org/10.1016/0012-821X(89)90151-9

Mishra, D. C., Chandra Sekhar, D. V., Venkata Raju, D. C., & Vijaya Kumar, V. (1999). Crustal structure based on gravity–magnetic modelling constrained from seismic studies under Lambert Rift, Antarctica and Godavari and Mahanadi rifts, India and their interrelationship. *Earth and Planetary Science Letters*, *172*(3–4), 287–300. https://doi.org/10.1016/S0012-821X(99)00212-5

Mittal, T., & Richards, M. A. (2021). The Magmatic Architecture of Continental Flood Basalts: 2. A New Conceptual Model. *Journal of Geophysical Research: Solid Earth*, *126*(12), e2021JB021807. https://doi.org/10.1029/2021JB021807

Mittal, T., Richards, M. A., & Fendley, I. M. (2021). The Magmatic Architecture of Continental Flood Basalts I: Observations From the Deccan Traps. *Journal of Geophysical Research: Solid Earth*, *126*(12). https://doi.org/10.1029/2021JB021808

Morgan, J. P., & Smith, W. H. F. (1992). Flattening of the sea-floor depth-age curve as a response to asthenospheric flow. *Nature*, *359*(6395), 524–527. https://doi.org/10.1038/359524a0

Müller, R. D., Yatheesh, V., & Shuhail, M. (2015). The tectonic stress field evolution of India since the Oligocene. *Gondwana Research*, *28*(2), 612–624. https://doi.org/10.1016/J.GR.2014.05.008

Neuharth, D., Brune, S., Wrona, T., Glerum, A., Braun, J., & Yuan, X. (2022). Evolution of Rift Systems and Their Fault Networks in Response to Surface Processes. *Tectonics*, *41*(3), e2021TC007166. https://doi.org/10.1029/2021TC007166

Neuharth, D., Brune, S., Glerum, A., Morley, C. K., Yuan, X., & Braun, J. (2022). Flexural strike-slip basins. *Geology*, *50*(3), 361–365. https://doi.org/10.1130/G49351.1

Pandey, O. P., Agrawal, P. K., & Negi, J. G. (1996). Evidence of low density sub-crustal underplating beneath western continental region of India and adjacent Arabian Sea: Geodynamical considerations. *Journal of Geodynamics*, *21*(4), 365–377. https://doi.org/10.1016/0264-3707(95)00036-4

Pons, M., Sobolev, S. V., Liu, S., & Neuharth, D. (2022). Hindered Trench Migration Due To Slab Steepening Controls the Formation of the Central Andes. *Journal of Geophysical Research: Solid Earth*, *127*(12), e2022JB025229. https://doi.org/10.1029/2022JB025229

Radha Krishna, M., Verma, R. K., & Purushotham, A. K. (2002). Lithospheric structure below the eastern Arabian Sea and adjoining West Coast of India based on integrated analysis of gravity and seismic data. *Marine Geophysical Researches*, *23*(1), 25–42. https://doi.org/10.1023/A:1021288003781/METRICS

Radhakrishna, B. P. (1993). Neogene uplift and geomorphic rejuvenation of the Indian Peninsula. *Current Science*, *Vol. 64, No. 11/12*(Special Issue), 787–793. https://doi.org/https://www.jstor.org/stable/24096189

Raju, D. S. N. (2008). Stratigraphy of India. *ONGC Bull., Spec. Issue*, *(43), 1*.

Rao, B. R., & Rao, P. S. (1984). Historical seismicity of Peninsular India. *Bulletin of the Seismological Society of America*, *74*(6), 2519–2533. https://doi.org/10.1785/BSSA0740062519

Rao, D. G., Krishna, K. S., & Sar, D. (1997). Crustal evolution and sedimentation history of the Bay of Bengal since the Cretaceous. *Journal of Geophysical Research: Solid Earth*, *102*(B8), 17747–17768. https://doi.org/10.1029/96JB01339

Rao, G. S., Radhakrishna, M., Sreejith, K. M., Krishna, K. S., & Bull, J. M. (2016). Lithosphere structure and upper mantle characteristics below the Bay of Bengal. *Geophysical Journal International*, *206*(1), 675–695. https://doi.org/10.1093/GJI/GGW162

Richards, F. D., Hoggard, M. J., & White, N. J. (2016). Cenozoic epeirogeny of the Indian peninsula. *Geochemistry, Geophysics, Geosystems*, *17*(12), 4920–4954. https://doi.org/10.1002/2016GC006545

Roger Buck, W. (1986). Small-scale convection induced by passive rifting: the cause for uplift of rift shoulders. *Earth and Planetary Science Letters*, *77*(3–4), 362–372. https://doi.org/10.1016/0012-821X(86)90146-9

Rogers, K. G., & Goodbred, S. L. (2014). The Sundarbans and Bengal Delta: The World's Largest Tidal Mangrove and Delta System. *World Geomorphological Landscapes*, 181–187. https://doi.org/10.1007/978-94-017-8029-2_18

Roy, A., Mandal, N., & Van Hunen, J. (2024). Dynamic evolution of competing same-dip double subduction: New perspectives of the Neo-Tethyan plate tectonics. *Earth and Planetary Science Letters*, *647*, 119032. https://doi.org/10.1016/J.EPSL.2024.119032

Roy, A. B., & Chatterjee, A. (2015). Tectonic framework and evolutionary history of the Bengal Basin in the Indian subcontinent. *Current Science*, *9*(2), 271–279. https://doi.org/https://www.jstor.org/stable/24905853

Roy, Sunil K., Kumar, M. R., Kanaujia, J., Gupta, S., Singh, B., Mandal, P., & Srinagesh, D. (2024). Insights into the mechanisms forging seismic anisotropy in the upper mantle beneath India. *Tectonophysics*, *888*, 230454. https://doi.org/10.1016/J.TECTO.2024.230454

Roy, Sunil Kumar, Srinagesh, D., Saikia, D., Singh, A., & Kumar, M. R. (2012). Seismic anisotropy beneath the Eastern Dharwar craton. *Lithosphere*, *4*(4), 259–268. https://doi.org/10.1130/L198.1

Royden, L. H., Burchfiel, B. C., & Van Der Hilst, R. D. (2008). The geological evolution of the Tibetan plateau. *Science*, *321*(5892), 1054–1058. https://doi.org/10.1126/SCIENCE.1155371/ASSET/85943FBF-8019-422F-8691-6BDF90923918/ASSETS/GRAPHIC/321_1054_F6.JPEG

Ruetenik, G. A., Moucha, R., & Hoke, G. D. (2016). Landscape response to changes in dynamic topography. *Terra Nova*, *28*(4), 289–296. https://doi.org/10.1111/TER.12220

Russo, R. M., & Silver, P. G. (1994). Trench-Parallel Flow Beneath the Nazca Plate from Seismic Anisotropy. *Science*, *263*(5150), 1105–1111. https://doi.org/10.1126/SCIENCE.263.5150.1105

Saha, G. K., Prakasam, K. S., & Rai, S. S. (2020). Diversity in the peninsular Indian lithosphere revealed from ambient noise and earthquake tomography. *Physics of the Earth and Planetary Interiors*, *306*, 106523. https://doi.org/10.1016/J.PEPI.2020.106523

Saha, G. K., Rai, S. S., Prakasam, K. S., & Gaur, V. K. (2021). Distinct lithospheres in the Bay of Bengal inferred from ambient noise and earthquake tomography. *Tectonophysics*, *809*, 228855. https://doi.org/10.1016/J.TECTO.2021.228855

Sandiford, D., & Moresi, L. (2019). Improving subduction interface implementation in dynamic numerical models. *Solid Earth*, *10*(3), 969–985. https://doi.org/10.5194/SE-10-969-2019

Sandiford, D., Moresi, L., Sandiford, M., & Yang, T. (2019). Geometric controls on flat slab seismicity. *Earth and Planetary Science Letters*, *527*, 115787. https://doi.org/10.1016/J.EPSL.2019.115787

Sen, J., Roy, A., & Mandal, N. (2024). Decoding the Eastward Tilt of the Indian Peninsular Plateau: Insights from Geodynamic Modelling [Dataset]. https://doi.org/10.5281/ZENODO.14416339

Sribin, C., Padma Rao, B., Rohilla, S., & Jha, K. (2024). Crustal structure beneath the Western Dharwar Craton segment of Western Ghats: Insights from ambient noise correlation technique. *Journal of Asian Earth Sciences*, *272*, 106240. https://doi.org/10.1016/J.JSEAES.2024.106240

Steckler, M. S., Mondal, D. R., Akhter, S. H., Seeber, L., Feng, L., Gale, J., et al. (2016). Locked and loading megathrust linked to active subduction beneath the Indo-Burman Ranges. *Nature Geoscience 2016 9:8*, *9*(8), 615–618. https://doi.org/10.1038/ngeo2760

Stolar, D., Roe, G., & Willett, S. (2007). Controls on the patterns of topography and erosion rate in a critical orogen. *Journal of Geophysical Research: Earth Surface*, *112*(4). https://doi.org/10.1029/2006JF000713

Subrahmanyam, C., & Chand, S. (2006). Evolution of the passive continental margins of India—a geophysical appraisal. *Gondwana Research*, *10*(1–2), 167–178. https://doi.org/10.1016/J.GR.2005.11.024

Thorne, R. L., Roberts, S., & Herrington, R. (2012). Climate change and the formation of nickel laterite deposits. *Geology*, *40*(4), 331–334. https://doi.org/10.1130/G32549.1

Tiwari, P. K., Surve, G., & Mohan, G. (2006). Crustal constraints on the uplift mechanism of the Western Ghats of India. *Geophysical Journal International*, *167*(3), 1309–1316. https://doi.org/10.1111/J.1365-246X.2006.03093.X/3/167-3-1309-FIG008.JPEG

Tucker, G. E. (2015). Landscape evolution. *Crustal and Lithosphere Dynamics: Treatise on Geophysics, Edited by: Watts, AB, Elsevier*, 593–630.

Tucker, G. E., & Hancock, G. R. (2010). Modelling landscape evolution. *Earth Surface Processes and Landforms*, *35*(1), 28–50. https://doi.org/10.1002/ESP.1952

Valdiya, K. S. (2001). Tectonic resurgence of the Mysore plateau and surrounding regions in cratonic Southern India. *Current Science*, *Vol.81, No.8*, 1068–1089. https://doi.org/https://www.jstor.org/stable/24106531

Veeraswamy, K., & Raval, U. (2005). Remobilization of the palaeoconvergent corridors hidden under the Deccan trap cover and some major stable continental region earthquakes. *Current Science*, *89*(3), 522–530.

Vita-Finzi, C. (2004). Buckle-controlled seismogenic faulting in peninsular India. *Quaternary Science Reviews*, *23*(23–24), 2405–2412. https://doi.org/10.1016/J.QUASCIREV.2004.01.008

Watts, A. B., & Cox, K. G. (1989). The Deccan Traps: an interpretation in terms of progressive lithospheric flexure in response to a migrating load. *Earth and Planetary Science Letters*, *93*(1), 85–97. https://doi.org/10.1016/0012-821X(89)90186-6

Weissel, J. K., & Karner, G. D. (1989). Flexural uplift of rift flanks due to mechanical unloading of the lithosphere during extension. *Journal of Geophysical Research: Solid Earth*, *94*(B10), 13919–13950. https://doi.org/10.1029/JB094IB10P13919

Whipple, K. X., & Meade, B. J. (2004). Controls on the strength of coupling among climate, erosion, and deformation in two-sided, frictional orogenic wedges at steady state. *Journal of Geophysical Research: Earth Surface*, *109*(F1). https://doi.org/10.1029/2003JF000019

Whipple, Kelin X. (2009). The influence of climate on the tectonic evolution of mountain belts. *Nature Geoscience 2009 2:2*, *2*(2), 97–104. https://doi.org/10.1038/ngeo413

White, R., & McKenzie, D. (1989). Magmatism at rift zones: The generation of volcanic continental margins and flood basalts. *Journal of Geophysical Research: Solid Earth*, *94*(B6), 7685–7729. https://doi.org/10.1029/JB094IB06P07685

Whiting, B. M., Karner, G. D., & Driscoll, N. W. (1994). Flexural and stratigraphic development of the west Indian continental margin. *Journal of Geophysical Research: Solid Earth*, *99*(B7), 13791–13811. https://doi.org/10.1029/94JB00502

Widdowson, M., & Cox, K. G. (1996). Uplift and erosional history of the Deccan Traps, India: Evidence from laterites and drainage patterns of the Western Ghats and Konkan Coast. *Earth and Planetary Science Letters*, *137*(1–4), 57–69. https://doi.org/10.1016/0012-821X(95)00211-T

Widdowson, M., & Mitchell, C. (1999). Large-scale stratigraphical, structural and geomorphological constraints for earthquakes in the Southern Deccan Traps, India: The case for denudationally-driven seismicity. *Mem. Geol. Soc. India*, *43(1)*, 425–452.

Yamato, P., Husson, L., Becker, T. W., & Pedoja, K. (2013). Passive margins getting squeezed in the mantle convection vice. *Tectonics*, *32*(6), 1559–1570. https://doi.org/10.1002/2013TC003375

Figure Captions

Figure 1: Eastward river flow patterns in Indian peninsula (IP). The major rivers shown here include Narmada (Nar), Tapi (Tap), Godavari (God), Bhima (Bhi), Krishna (Kri), Tungabhadra (Tun), Cauvery (Cau), Ponnaiyar (Pon), Palar (Pal), Mahanadi (Mah), Tel (Tel), Indravati (Ind), Bhavani (Bha), Pennar (Pen), and Kollidam (Kol). The river system extends from the Arabian Sea on the west to the Bay of Bengal on the east, constituting the main regional water resources in IP. The eastward decrease in topographic elevation grossly conforms to the river flow directions. The drainage system depicted in the map excludes extra peninsular rivers. The map is developed by using the Generic Mapping Tools (GMT).

Figure 2: Tectonic setting of the Indian Peninsular (IP) landmass, constituted by major tectonic plates: the Indian Plate, surrounded by the Arabian Plate to the west, the Eurasian Plate to the north, and the Indo-Australian Plate to the east, and the plate boundaries: the Carlsberg Ridge, the Mid-Indian Ridge, and the Sunda Trench. The IP continental craton consists of large-scale geomorphic elements: the Western Ghats, the Eastern Ghats Mountain

ranges, and the Deccan Plateau. Seafloor age data indicates contrasting ages of oceanic lithosphere beneath the Bay of Bengal (~140 Ma) and the Arabian Sea (~ 40 Ma).

Figure 3: (a) A set of topographic profiles (P1–P6) across the Indian Peninsular landmass, displaying eastward decrease in topographic elevations (in meters), forming first-order surface slopes to east (red dashed line). It is noteworthy that the surface slope varies from 0.008° to 0.1° in the south direction. The profile locations: P1–P6 are shown in (b). (c) DEM model calculated plot showing a steep increase in the topographic slopes from north to south.

Figure 4: Strongly asymmetric topographic profiles (S1–S8) across the Western Ghats escarpment. The escarpment exhibit elevation drops of more than 1000 m, forming steep slopes (70° to 82°) to west, and a much gentler eastward slope (40° to 15°) on the other side.

Figure 5: (a) Two-dimensional thermo-mechanical model setup that represents an E-W vertical section of Indian peninsula. The model consists of a continental block, flanked by oceanic blocks and a sticky air layer at the top. Periodic boundary conditions are imposed at the lateral walls, while a no-slip boundary condition at the model base. The colour scale indicates the viscosity distribution. (b) Depth-dependent variations of temperature (yellow) and viscosity (gray) of (i) oceanic, and (ii) continental lithosphere, and (iii) the yield strength considered in this model. It is to be noted that the temperature increases with depth, reaching ~1500°C at the lithospheric base, accompanied by a significant viscosity decrease in the asthenosphere.

Figure 6: Topographic map of the Indian subcontinent, including the Arabian Sea and the Bay of Bengal (BOB) of varying sea-floor ages (in millions of years, Ma). The colour bar denotes the age spectrum, ranging from 0 Ma (recent) to over 140 Ma (oldest). It is noteworthy that the oceanic lithosphere beneath the BOB is significantly older than that beneath the Arabian Sea. Horizontal lines (A–B, C–D, and E–F) represent the cross-sections of varying continental width (L) considered for the thermomechanical model simulations (right panels). Colour bar shows viscosity values on a logarithmic scale chosen in the model. P_1-P_5 are the positions of the tracers at the surface of the lithospheric block, which are used to track the surface displacement.

Figure 7: (a) A time series presentation of the thermo-mechanical model simulations for the E-W transect (A-B) in the northern segment of Indian peninsula (NIP). The isotherms reveal variations in temperatures in the NIP model lithosphere, including the Arabian Sea (AS), and the Bay of Bengal (BOB). (b)Topographic evolution in the same model simulation by differential surface uplift. The topography is reconstructed from progressive vertical displacements of five tracer points: P_1 to P_5, as explained in the caption of Fig. 6. At $t = 0$ Myr, the topography is flat, which gains slopes of 0.2° and 0.3° at model run times: $t = 0.1$ Myr and 0.2 Myr, respectively.

Figure 8: (a) Thermo-mechanical model simulations for the Central Peninsular India (CIP) ($L = 750$ km), including the adjoining Arabian Sea (AS) and Bay of Bengal (BOB). The isotherm concentrations indicate varying thermal gradients in the continental and oceanic lithosphere. (b) Topographic evolution in the IP continental lithosphere. The initially ($t = 0$) flat model surface undergoes differential uplift to produce slopes of 0.2°, and 0.4° at model run times: $t = 0.1$, and 0.2 Myr.

Figure 9: (a) Thermo-mechanical model simulations for the Southern Indian peninsula (SIP) ($L= 600$ km). (b) Topographic evolution in the PI lithospheric block. It is to be noted that the

model produces significantly steeper eastward surface slopes: 0.3° to 0.49° than the NIP and CIP models at the model run times: 0.1 Myr, and 0.2 Myr, respectively. In addition, the topography becomes more asymmetric.

Figure 10: IP model simulations showing sublithospheric mantle flow patterns and their interactions with the overlying lithosphere along three E-W transects: (a) NIP section, (b) CIP section, and SIP section. The models produce prominent westward sublithospheric flows, originated beneath the BOB, which eventually encounters the eastward flows originated beneath the AS, forming distinct upwelling zones at the western flank of the IP lithosphere. The reducing E-W continental width from north to south facilitates rotation of the continental lithospheric block, giving rise to greater topographic tilts in the southern sector.

Figure 11: (a) Graphical plots of the depths of top sediment surfaces and the crustal base (MOHO) in the Arabian Sea and the Bay of Bengal. The plots indicate a greater subsidence rate and sediment accumulation in the Bay of Bengal, correlating with deeper Moho depths, as compared to that in the Arabian Sea. (b) Sediment thickness map (in meters) across the Indian Ocean region, showing significantly thicker sediment columns in the Bay of Bengal (up to ~10,000 m), compared to that in the Arabian Sea (generally < 4000 m). Red arrows indicate east-west seismic anisotropy in the sublithospheric mantle, reflecting variations in mantle flow.

Figure 12: A 3D perspective of the asymmetric topography in Indian peninsula in relation to the model-generated sublithospheric mantle flows. The Western Ghats Escarpments lies above the upwelling zone in the mantle, implying the control of westward sub-lithospheric flows triggered by subsidence in the BOB lithosphere. The cross-section spans the SIP section (*L*= 600 km) along the Peninsular India.

Figure 1.

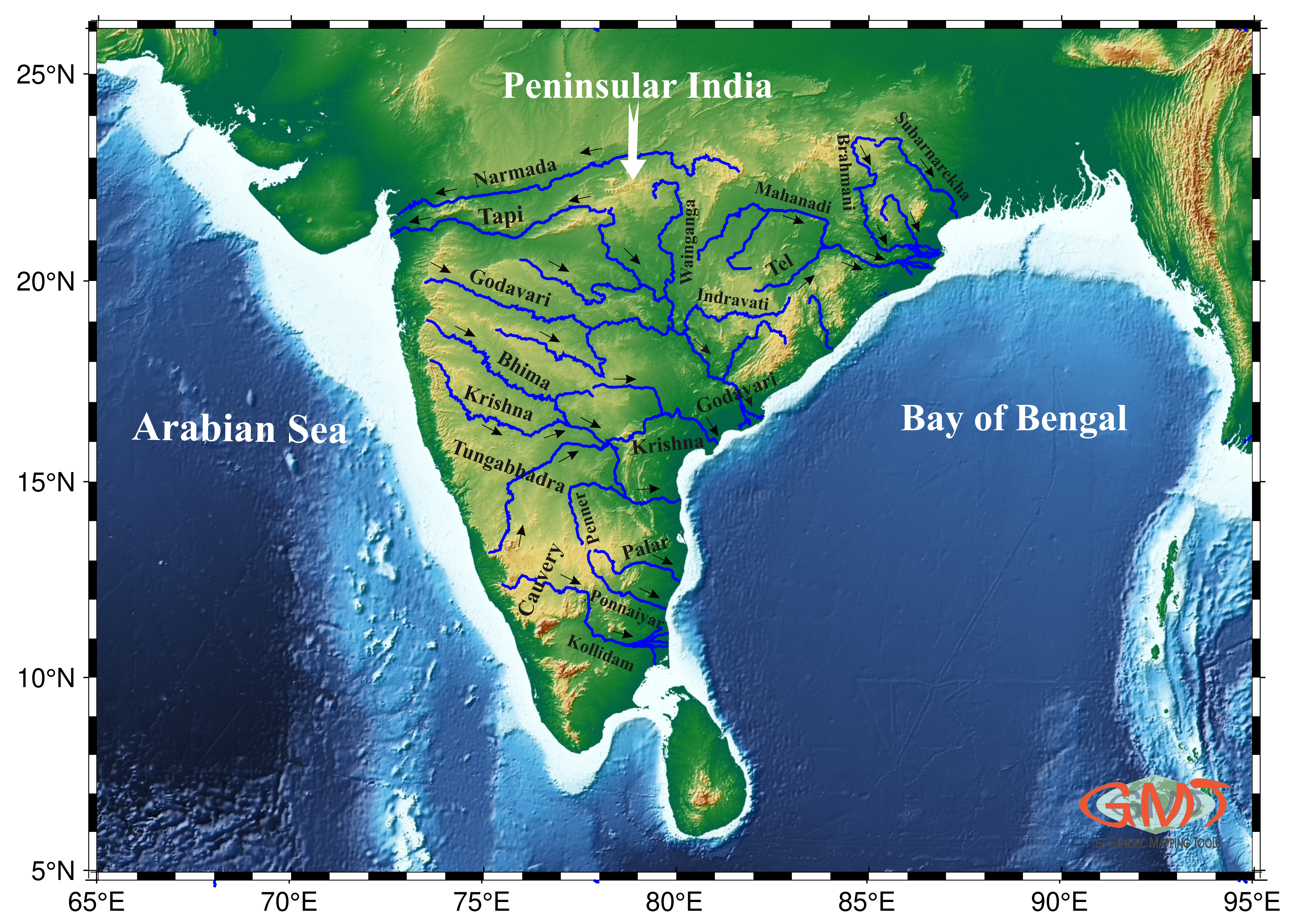
Peninsular India
Arabian Sea
Bay of Bengal
Narmada
Tapi
Godavari
Wainganga
Mahanadi
Brahmani
Subarnarekha
Tel
Indravati
Bhima
Krishna
Godavari
Krishna
Tungabhadra
Penner
Palar
Cauvery
Ponnaiyar
Kollidam
25°N
20°N
15°N
10°N
5°N
65°E
70°E
75°E
80°E
85°E
90°E
95°E

Figure 2.

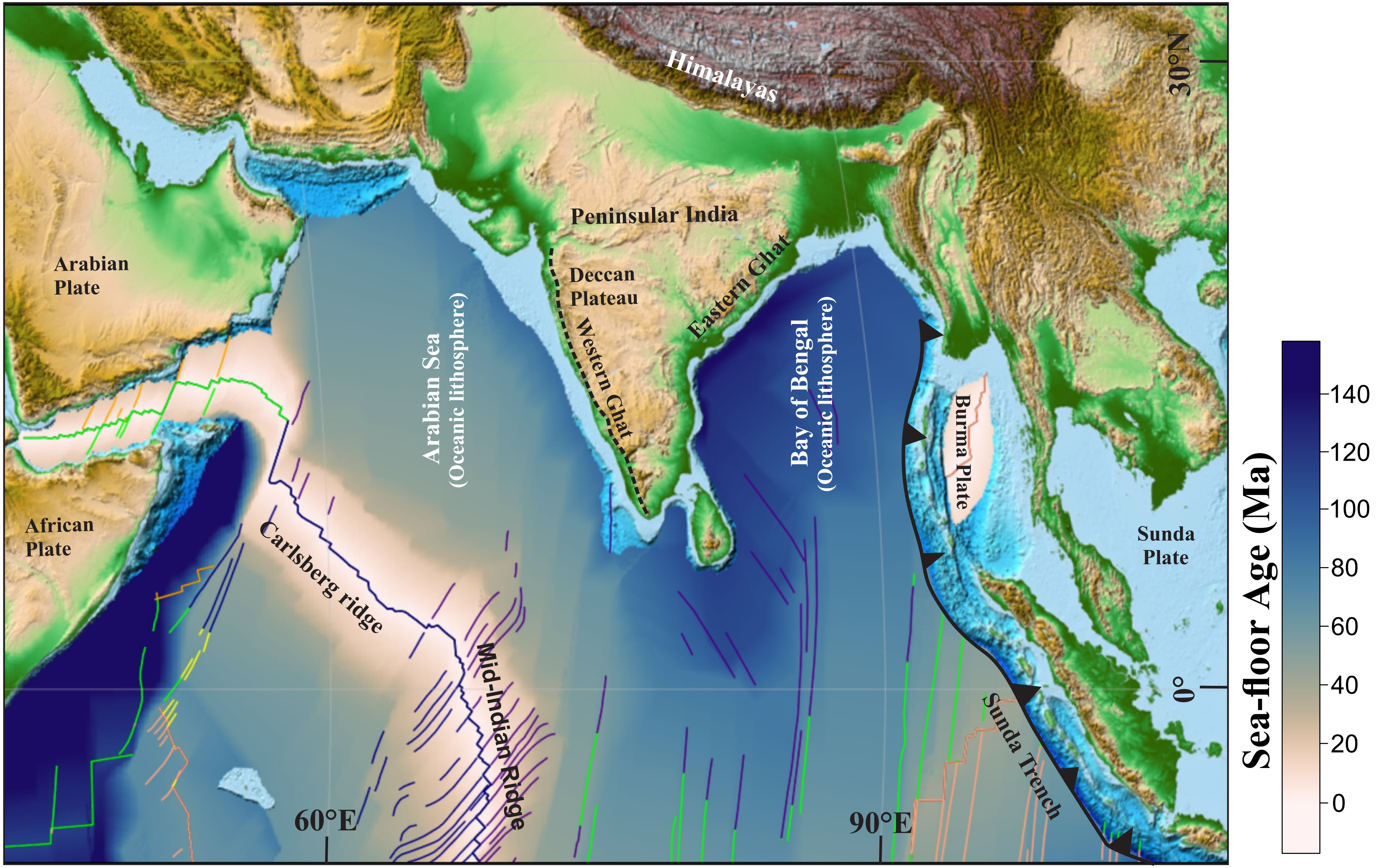
Himalayas
30°N
Peninsular India
Arabian Plate
Deccan Plateau
Eastern Ghat
Western Ghat
Arabian Sea (Oceanic lithosphere)
Bay of Bengal (Oceanic lithosphere)
Burma Plate
African Plate
Sunda Plate
Carlsberg ridge
Mid-Indian Ridge
Sunda Trench
0°
60°E
90°E
Sea-floor Age (Ma)
140
120
100
80
60
40
20
0

Figure 3.

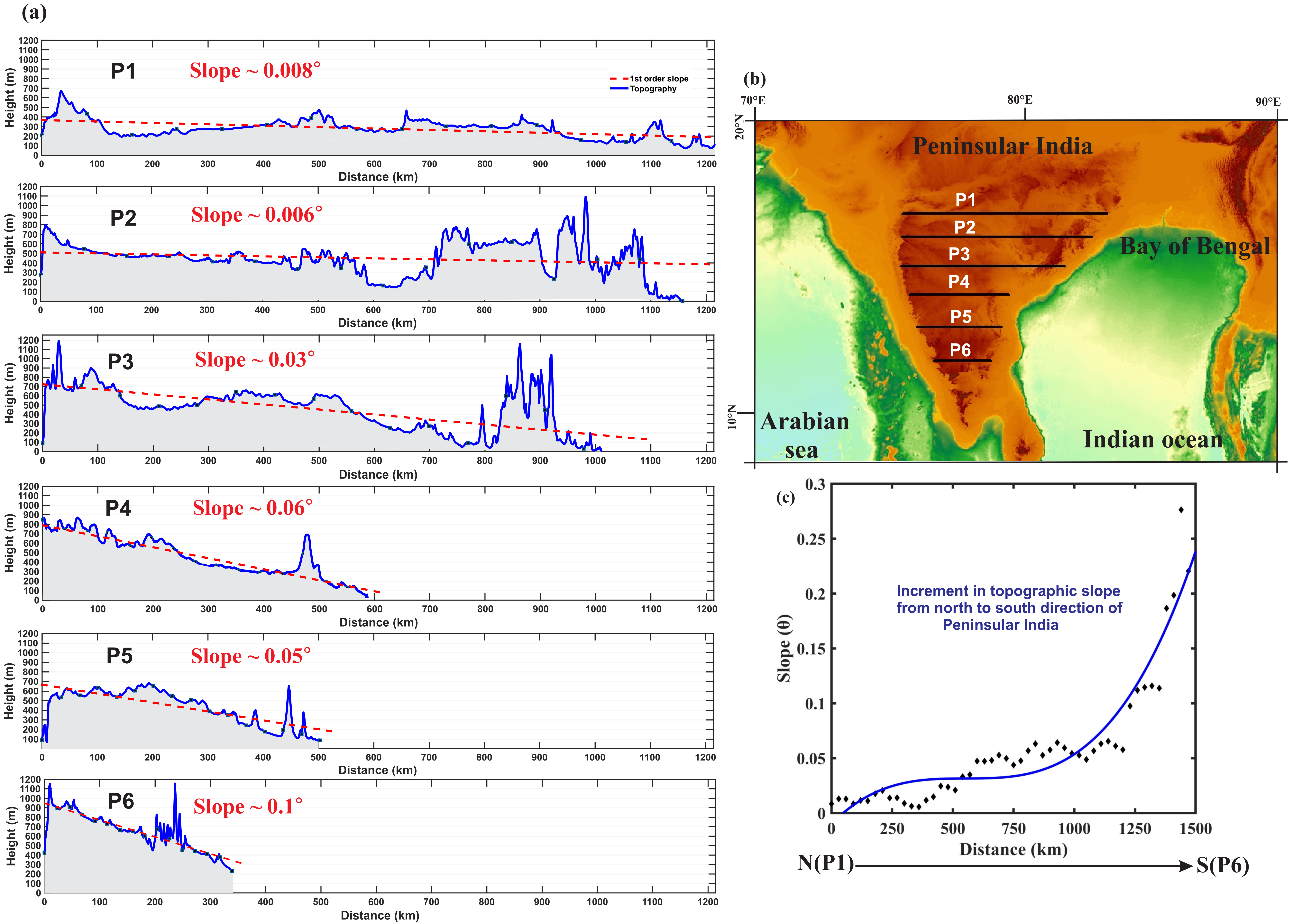

(a)
P1
Slope ~ 0.008°
1st order slope
Topography
P2
Slope ~ 0.006°
P3
Slope ~ 0.03°
P4
Slope ~ 0.06°
P5
Slope ~ 0.05°
P6
Slope ~ 0.1°
Height (m)
Distance (km)
(b)
70°E
80°E
90°E
20°N
10°N
Peninsular India
Bay of Bengal
Arabian sea
Indian ocean
(c)
Increment in topographic slope from north to south direction of Peninsular India
Slope (θ)
Distance (km)
N(P1)
S(P6)

Figure 4.

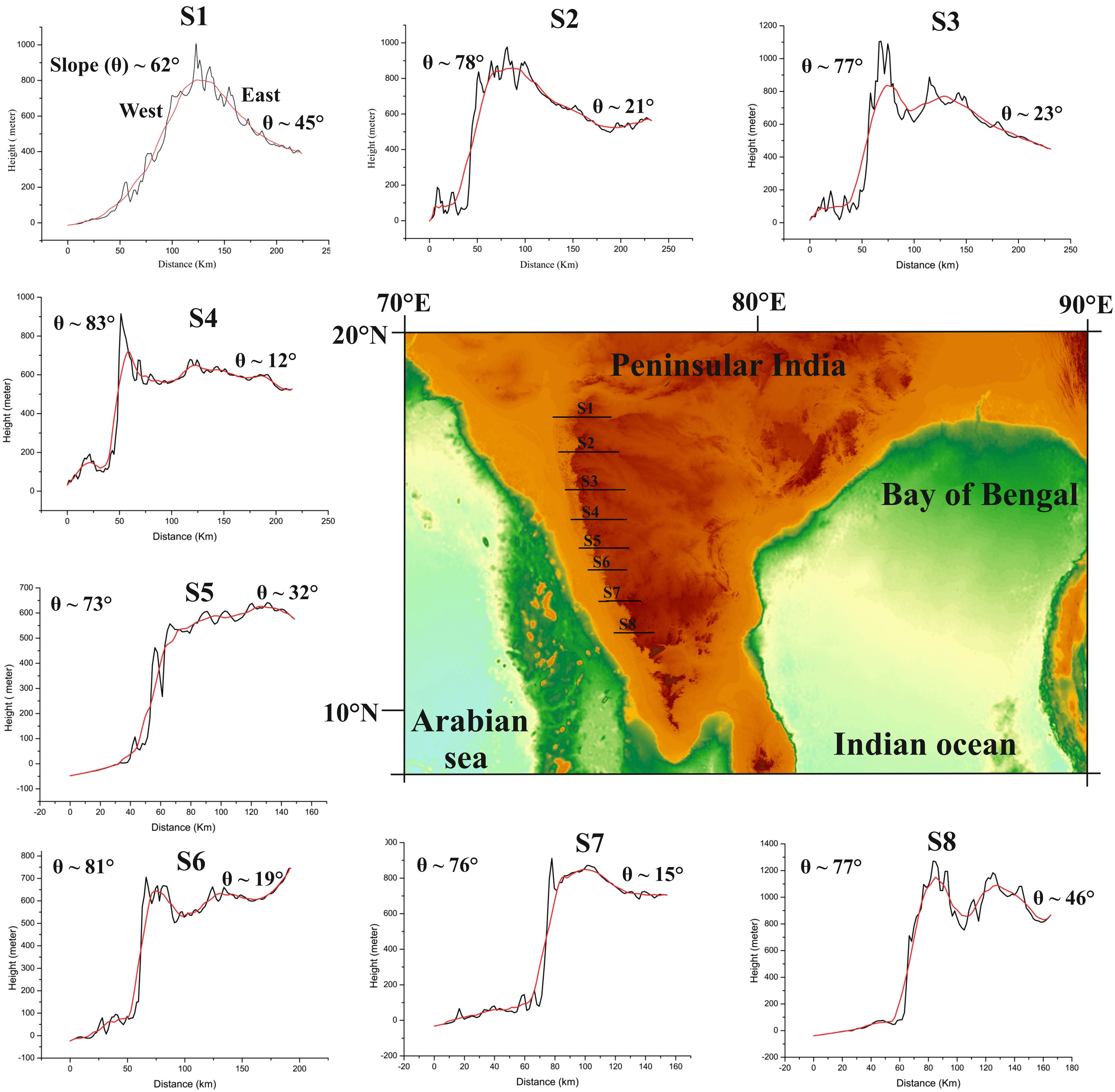

S1
Slope (θ) ~ 62°
West
East
θ ~ 45°
Height (meter)
Distance (Km)
S2
θ ~ 78°
θ ~ 21°
Height (meter)
Distance (Km)
S3
θ ~ 77°
θ ~ 23°
Height (meter)
Distance (km)
S4
θ ~ 83°
θ ~ 12°
Height (meter)
Distance (Km)
S5
θ ~ 73°
θ ~ 32°
Height (meter)
Distance (Km)
S6
θ ~ 81°
θ ~ 19°
Height (meter)
Distance (km)
S7
θ ~ 76°
θ ~ 15°
Height (meter)
Distance (km)
S8
θ ~ 77°
θ ~ 46°
Height (meter)
Distance (Km)
70°E
80°E
90°E
20°N
10°N
Peninsular India
Bay of Bengal
Arabian sea
Indian ocean

Figure 5.

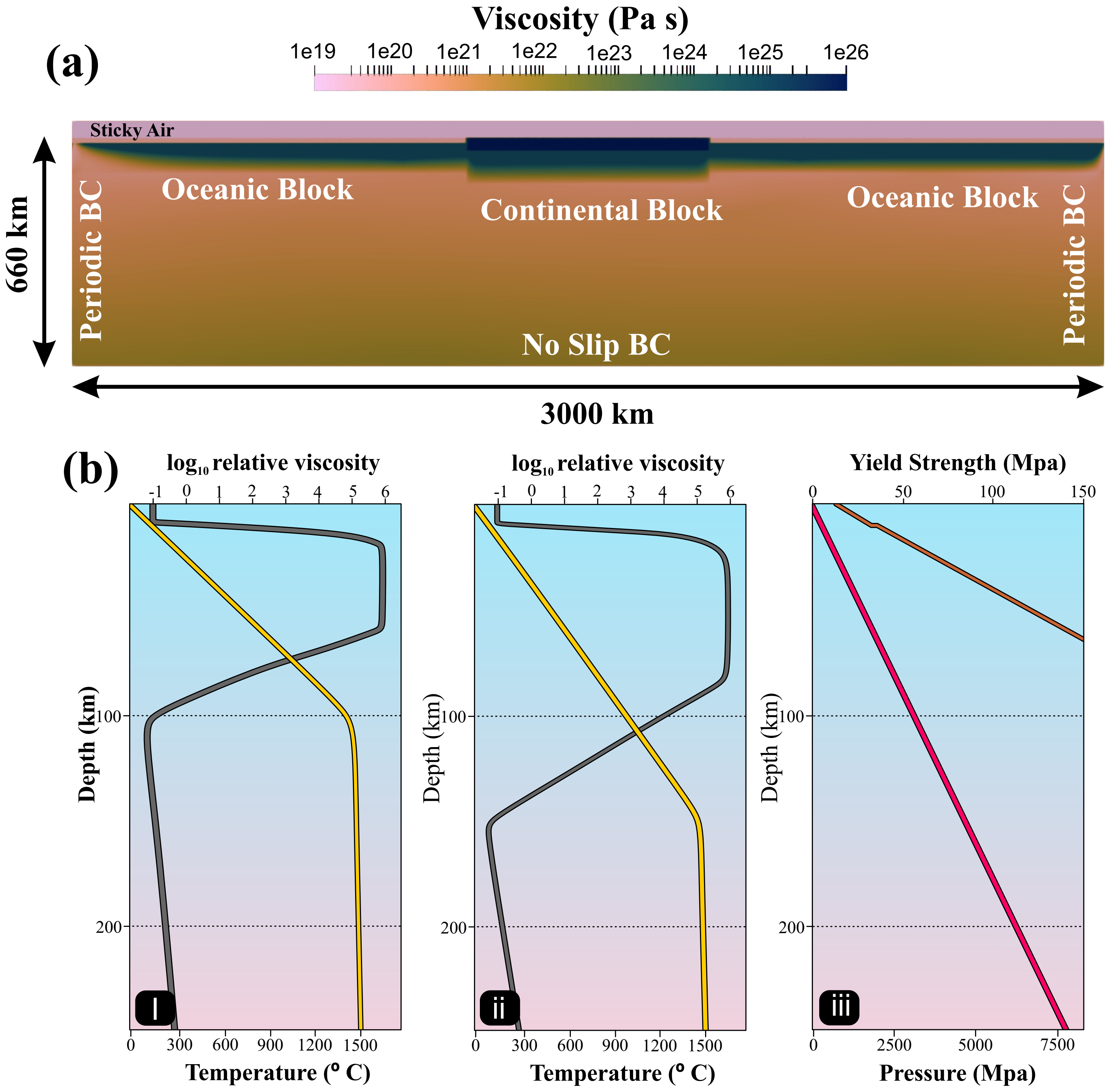

(a)
Viscosity (Pa s)
1e19
1e20
1e21
1e22
1e23
1e24
1e25
1e26
Sticky Air
Oceanic Block
Continental Block
Oceanic Block
Periodic BC
Periodic BC
No Slip BC
660 km
3000 km
(b)
log10 relative viscosity
-1
0
1
2
3
4
5
6
Depth (km)
100
200
Temperature (° C)
0
300
600
900
1200
1500
i
ii
Yield Strength (Mpa)
0
50
100
150
Pressure (Mpa)
2500
5000
7500
iii

Figure 6.

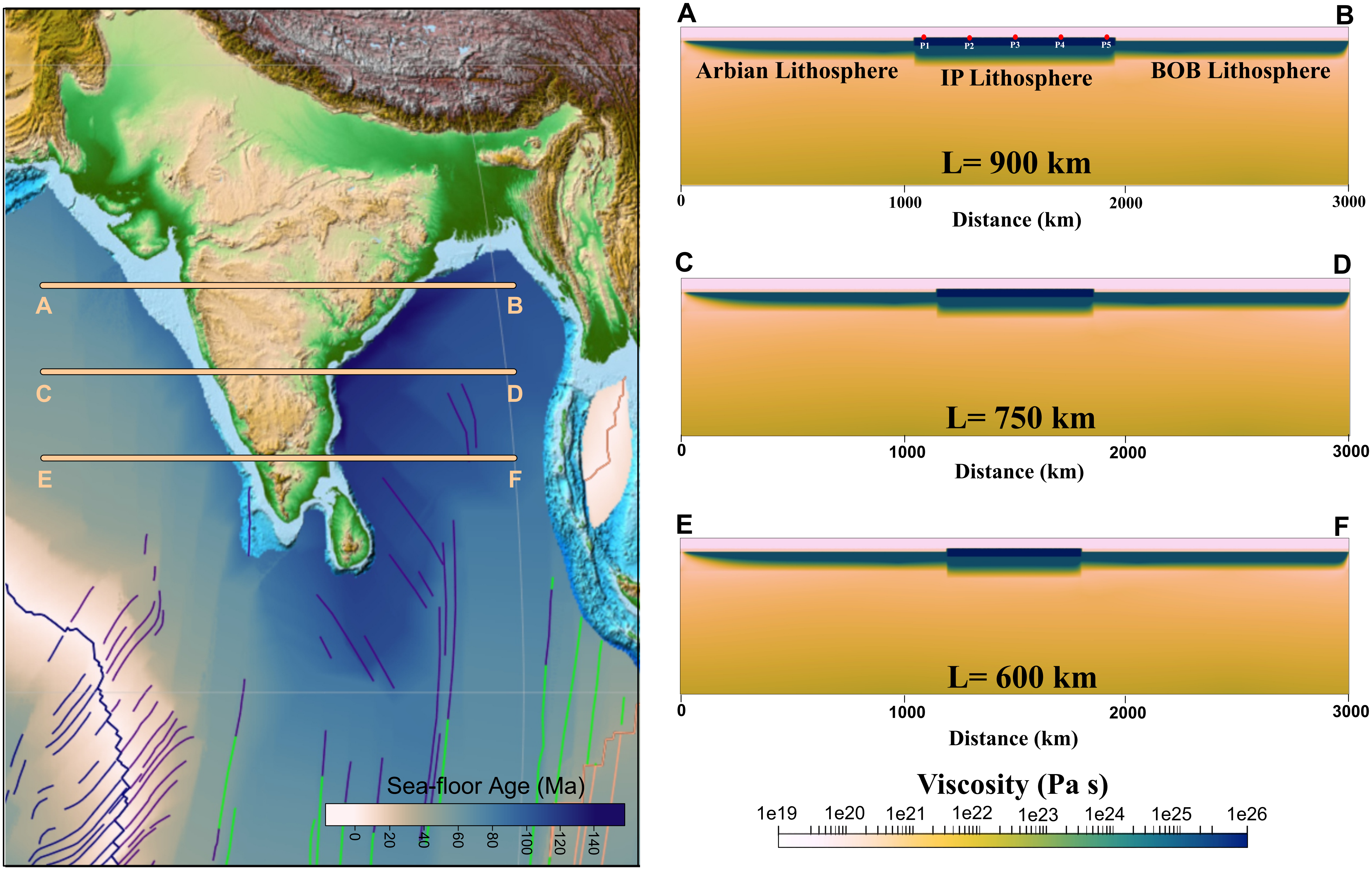

A
B
C
D
E
F
Sea-floor Age (Ma)
0
20
40
60
80
100
120
140
P1
P2
P3
P4
P5
Arbian Lithosphere
IP Lithosphere
BOB Lithosphere
L= 900 km
0
1000
2000
3000
Distance (km)
L= 750 km
L= 600 km
Viscosity (Pa s)
1e19
1e20
1e21
1e22
1e23
1e24
1e25
1e26

Figure 7.

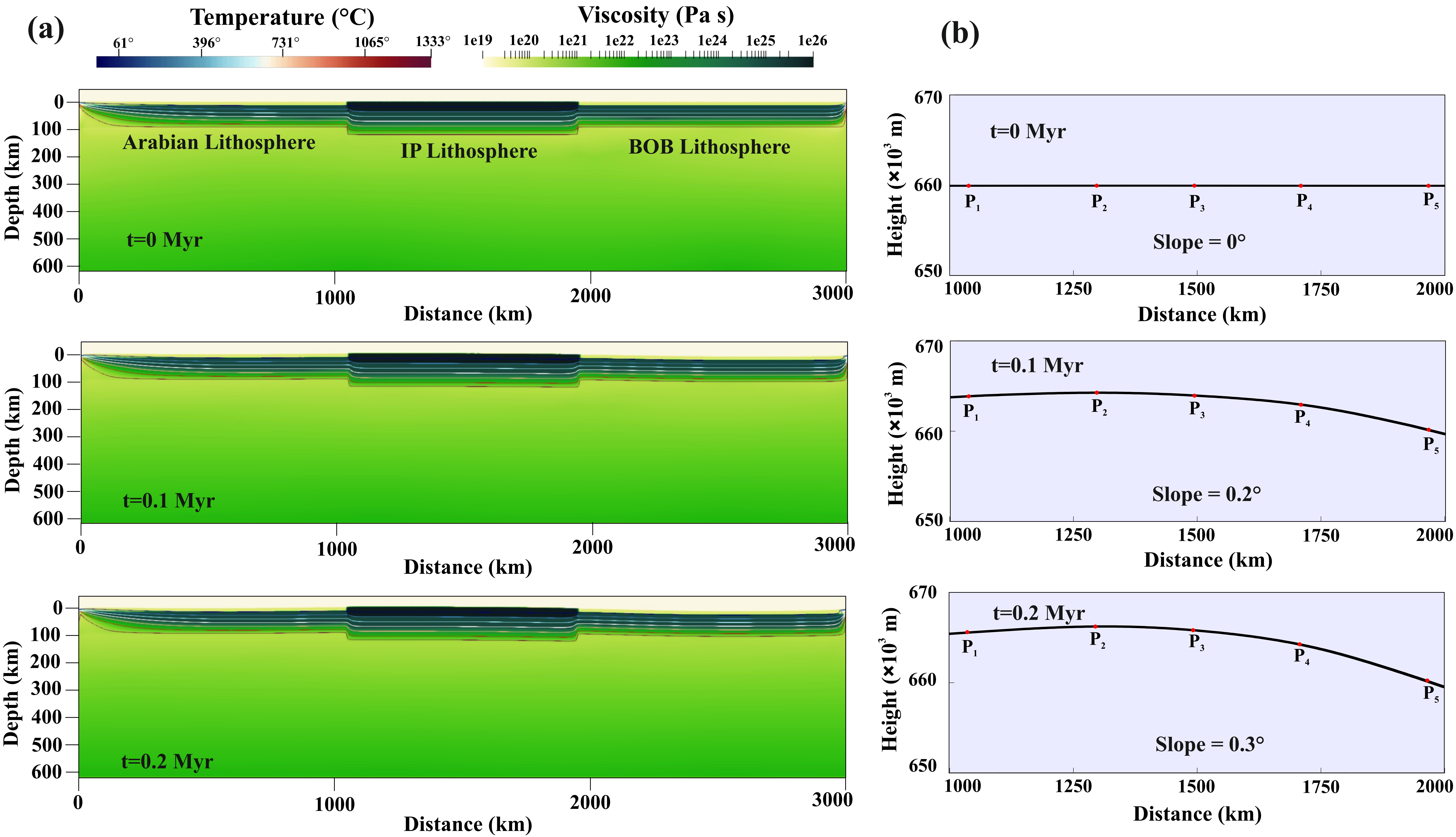

(a)
Temperature (°C)
61° 396° 731° 1065° 1333°
Viscosity (Pa s)
1e19 1e20 1e21 1e22 1e23 1e24 1e25 1e26
Arabian Lithosphere
IP Lithosphere
BOB Lithosphere
Depth (km)
Distance (km)
t=0 Myr
t=0.1 Myr
t=0.2 Myr
(b)
Height (×10³ m)
Slope = 0°
Slope = 0.2°
Slope = 0.3°
P1 P2 P3 P4 P5

Figure 8.

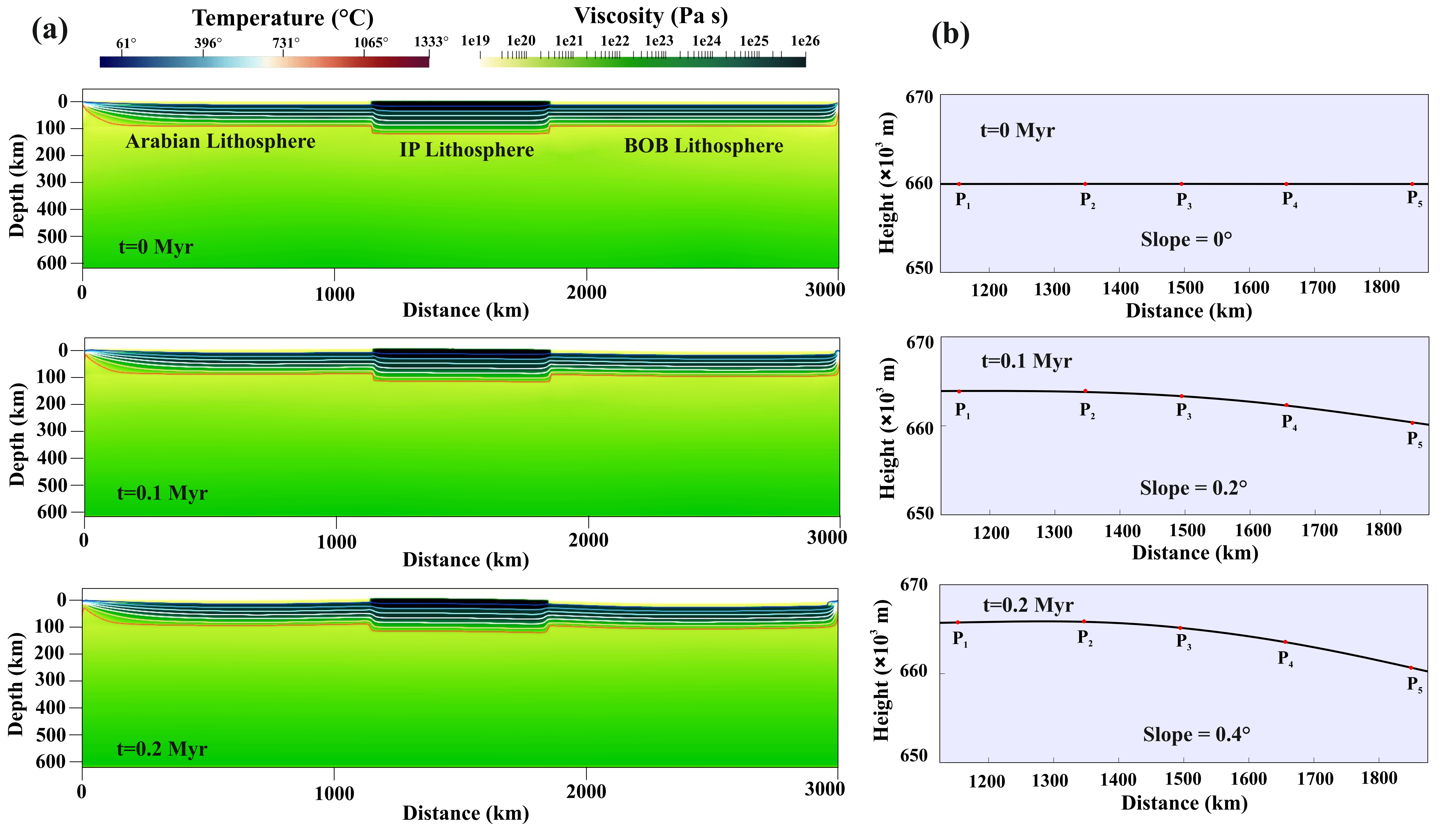

(a)
Temperature (°C)
61° 396° 731° 1065° 1333°
Viscosity (Pa s)
1e19 1e20 1e21 1e22 1e23 1e24 1e25 1e26
Arabian Lithosphere
IP Lithosphere
BOB Lithosphere
Depth (km)
Distance (km)
t=0 Myr
t=0.1 Myr
t=0.2 Myr
(b)
Height (×10^3 m)
Distance (km)
t=0 Myr
Slope = 0°
t=0.1 Myr
Slope = 0.2°
t=0.2 Myr
Slope = 0.4°
P1 P2 P3 P4 P5

Figure 9.

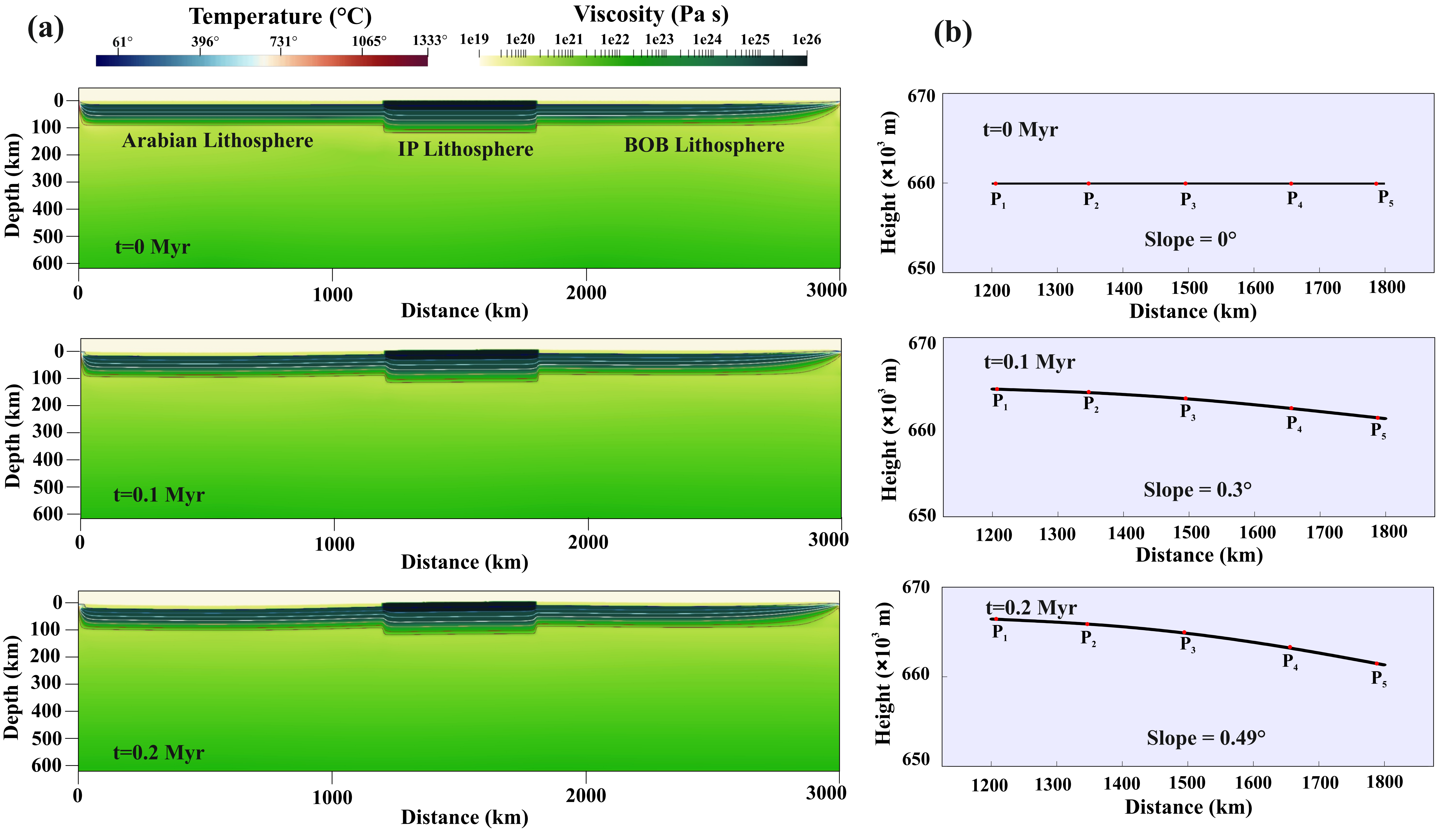
(a)
Temperature (°C)
61°
396°
731°
1065°
1333°
Viscosity (Pa s)
1e19
1e20
1e21
1e22
1e23
1e24
1e25
1e26
Arabian Lithosphere
IP Lithosphere
BOB Lithosphere
t=0 Myr
t=0.1 Myr
t=0.2 Myr
Depth (km)
Distance (km)
(b)
Height (×10³ m)
Slope = 0°
Slope = 0.3°
Slope = 0.49°
P1
P2
P3
P4
P5

Figure 10.

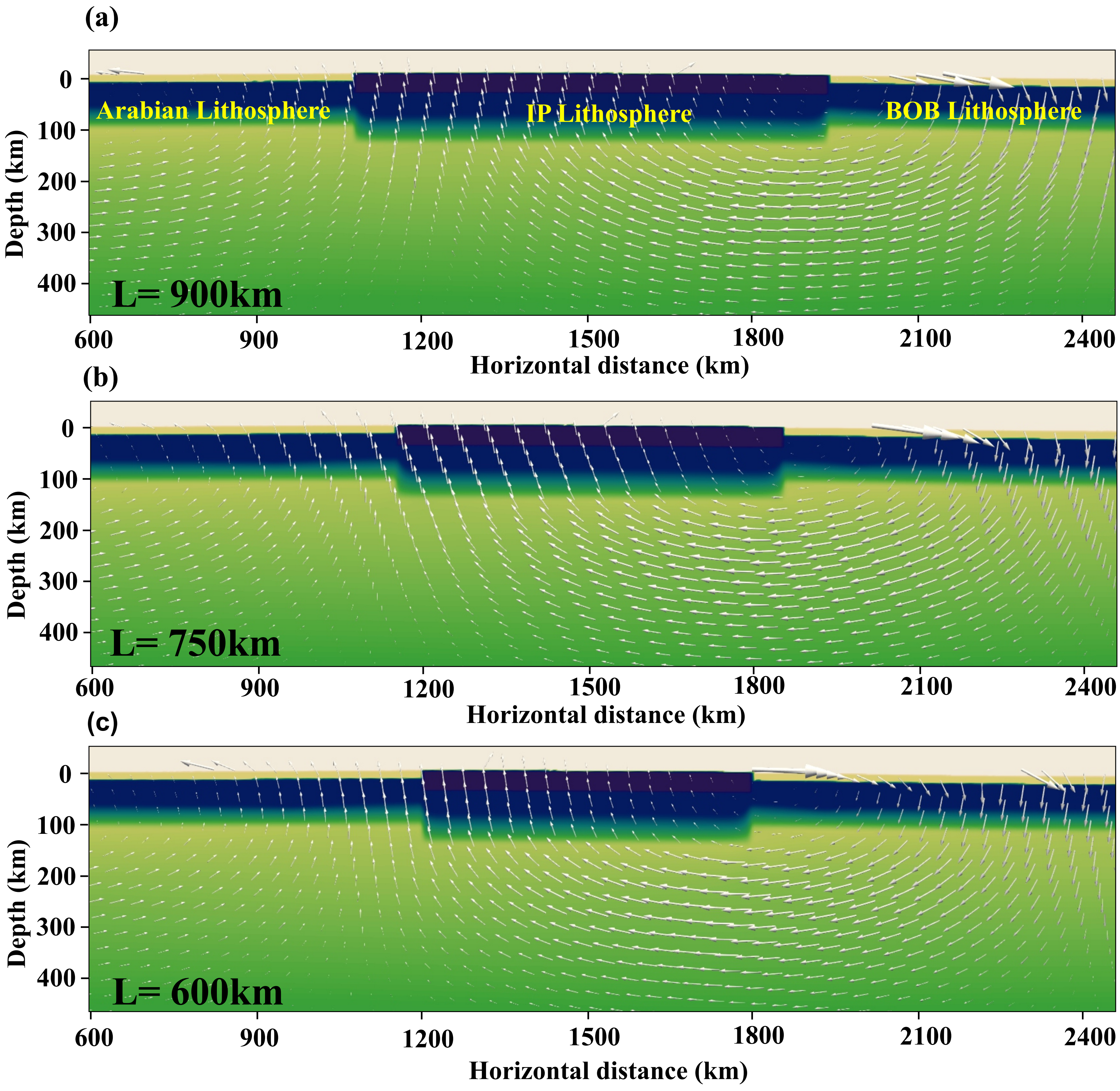

(a)
Arabian Lithosphere
IP Lithosphere
BOB Lithosphere
L= 900km
(b)
L= 750km
(c)
L= 600km
Depth (km)
Horizontal distance (km)

Figure 11.

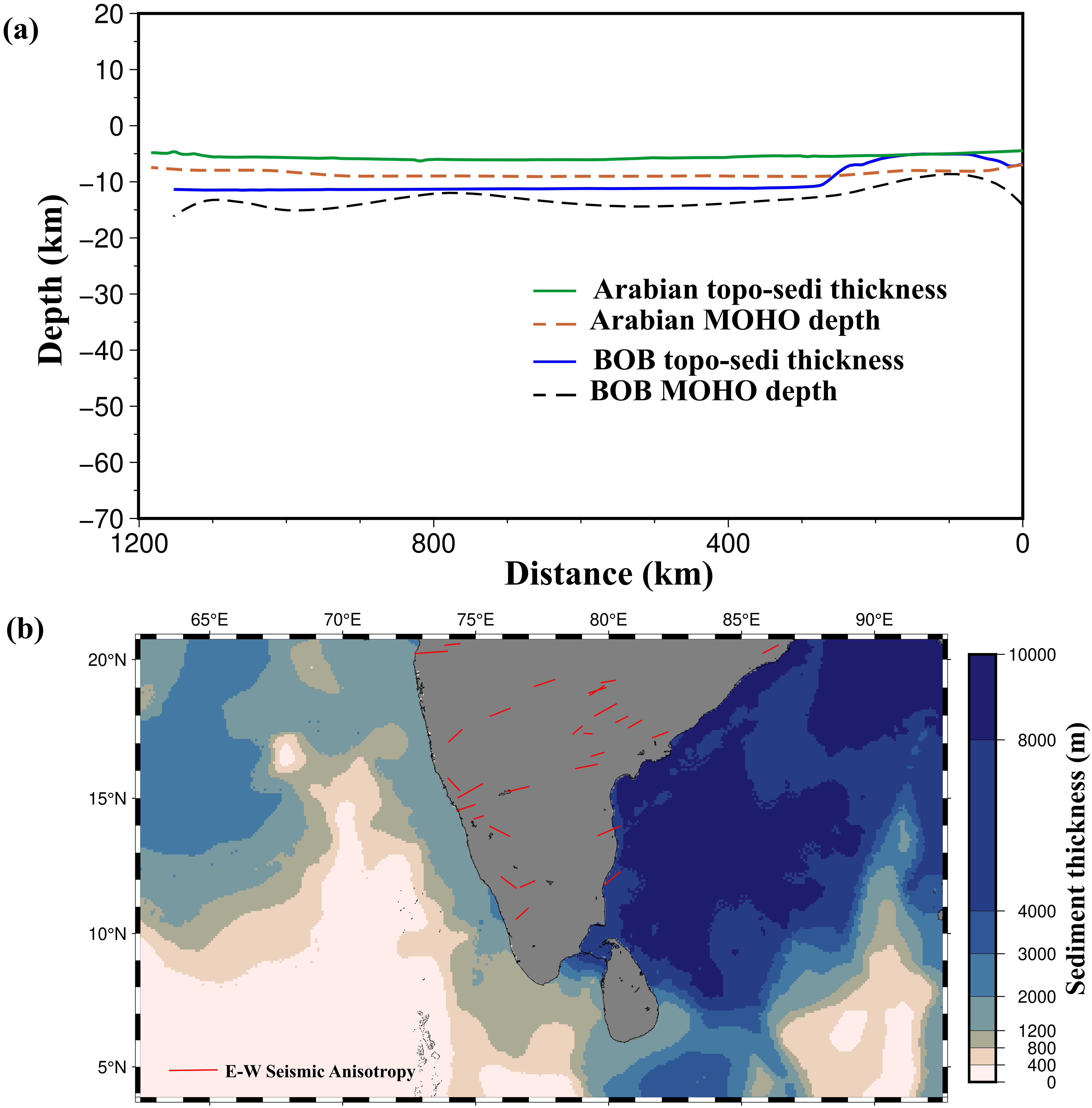
(a)
Depth (km)
Distance (km)
1200
800
400
0
20
10
0
−10
−20
−30
−40
−50
−60
−70
Arabian topo-sedi thickness
Arabian MOHO depth
BOB topo-sedi thickness
BOB MOHO depth
(b)
65°E
70°E
75°E
80°E
85°E
90°E
20°N
15°N
10°N
5°N
E-W Seismic Anisotropy
Sediment thickness (m)
10000
8000
4000
3000
2000
1200
800
400
0

Figure 12.

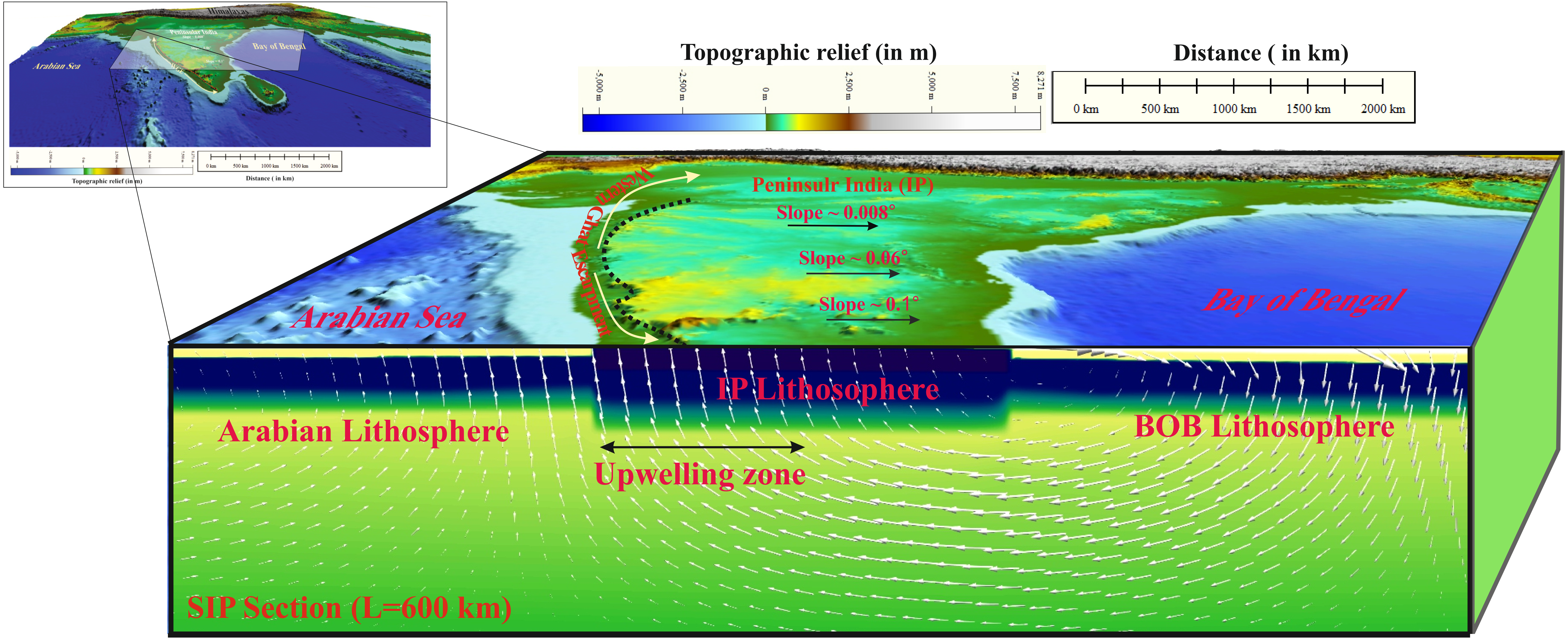
Himalayas
Peninsular India
Bay of Bengal
Arabian Sea
Topographic relief (in m)
Distance (in km)
Topographic relief (in m)
-5,000 m
-2,500 m
0 m
2,500 m
5,000 m
7,500 m
8,271 m
Distance (in km)
0 km
500 km
1000 km
1500 km
2000 km
Western Ghat Escarpment
Peninsulr India (IP)
Slope ~ 0.008°
Slope ~ 0.06°
Slope ~ 0.1°
Arabian Sea
Bay of Bengal
IP Lithosphere
Arabian Lithosphere
BOB Lithosphere
Upwelling zone
SIP Section (L=600 km)

Table 1: Model parameters used in thermo-mechanical model

Description	Symbol	Unit	Default Values
Thermal expansion coefficient	α	K^{-1}	3×10^{5}
Thermal diffusivity	κ	$m^2\ s^{-1}$	10^{-6}
Reference density	ρ_0	$kg\ m^{-3}$	3300
Surface temperature	T_s	K	273
Potential temperature	T_m	K	1673
Adiabatic temperature gradient	dT/dz	$K\ km^{-1}$	0.37
Gravitational acceleration	g	$m\ s^{-2}$	9.81
Maximum viscosity	η_{max}	Pa s	1.0×10^{26}
Minimum viscosity	η_{min}	Pa s	1.0×10^{19}
Crust viscosity	η_C	Pa s	1.0×10^{26}
Dislocation creep (Upper Mantle)			
Activation energy	E	$kJ\ mol^{-1}$	540
Activation volume	V	$cm^3\ mol^{-1}$	10
Pre-factor	A	$Pa^{n}\ s^{1}$	4.1×10^{15}
Exponent	n	-	3.5
Diffusion creep (Upper and Lower mantle)			
Activation energy	E	$kJ\ mol^{-1}$	300 (UM & LM)
Activation volume	V	$cm^3\ mol^{-1}$	4.5 (UM), 1.58 (LM)
Pre-factor	A	$Pa^{1}\ s^{1}$	1.87×10^{9} (UM)
			1.77×10^{14} (LM)
Exponent	n	-	1

Supplementary materials for

Decoding the Eastward Tilt of the Indian Peninsular Plateau: Insights from Geodynamic Modelling

Joyjeet Sen[1], Arnab Roy[2], Nibir Mandal[1*]
[1]Department of Geological Sciences, Jadavpur University, Kolkata 700032, India
[2]Department of Earth and Spatial Sciences, University of Idaho, Moscow 83844, USA
***Corresponding author: nibir.mandal@jadavpuruniversity.in**

S1. Geology of Peninsular India

Indian peninsular landmass comprises several Precambrian cratons, including the Dharwar, Singhbhum, Bundelkhand, and Bastar, which stabilized during the Archaean time through repeated tectonic cycles of magmatism, metamorphism, and crustal differentiation (Dey & Moyen, 2020; Jayananda et al., 2020, 2023; Saha & Mazumder, 2012) (Figure S1). The Dharwar Craton (DC), which is one of the oldest, geologically significant cratonic blocks is constituted by Archean rocks of ages spanning from 3.6 to 2.5 Ga (Chadwick et al., 2000; Brian Chadwick et al., 1997; Krapež et al., 2020; Prabhakar et al., 2009). The DC is divided into two parts: the Western Dharwar Craton (WDC) and the Eastern Dharwar Craton (EDC), separated by the Chitradurga shear zone (Figure S1). The WDC consists of low-grade greenstone belts, including volcanic and sedimentary sequences, and tonalite-trondhjemite-granodiorite (TTG) gneisses, which represent some of the Earth's earliest crust (Boraiaha, 2022; Ranjan et al., 2020; Wang et al., 2023). The EDC, in contrast, features high-grade gneisses, granitoids, and younger supracrustal rocks, indicating a more dynamic and thermally active evolution (Goswami et al., 2023; Mohan et al., 2013, 2020; Talukdar et al., 2018). The tectono-metamorphic history of the DC evolved through multiple episodes of crustal growth, accretion, and stabilization(Chadwick et al., 2000; Krapež et al., 2020; Prabhakar et al., 2009). The Singhbhum Craton (SC) is a spectacular Archaean block in eastern India, which is a mosaic of granitoids, greenstone belts, and banded iron formations (BIFs) belonging to the Iron Ore Group (Figure S1). The SC show evidence of tectonic and magmatic processes during the Mesoarchaean to Neoarchaean periods (Hofmann et al., 2022). The Bastar Craton (BC) in central India is an adjoining Precambrian craton, bordered by the Satpura Mobile Belt and the Eastern Ghats (Figure S1). The BC hosts ancient supracrustal sequences, such as the Sakoli and Sausar groups (Mohanty, 2021; Mondal et al., 2006; Saha & Deb, 2014), which have undergone significant metamorphism and deformation (Mohanty, 2021; Mondal et al., 2006; Saha & Deb, 2014).

These cratons collectively form the spatially vast basement of Indian Peninsula, intervened by isolated Proterozoic sedimentary basins, which are correlated with the rifting during breakup of the supercontinents: Columbia, Rodinia, and Gondwana. The Vindhyan, Cuddapah, and Chhattisgarh basins, known as "Purana basins", (Figure S1) hold sedimentary sequences deposited in rift-controlled environments (Bose et al., 2015; Miall et al., 2015; Singh &Mishra, 2002). The Vindhyan Basin, for instance, records over a billion years of sedimentation, including fluvial and shallow marine deposits, reflecting tectonic stability and prolonged sediment accumulation during the Mesoproterozoic to Neoproterozoic (Bose et al., 2015; Miall et al., 2015). The Eastern Ghats Mobile Belt (EGMB) represents one of the most tectonically active regions of Peninsular India (Figure S1), comprising high-grade metamorphic rocks, such as charnockites, khondalites, and granulites. The EGMB preserves evidence of Proterozoic collision and crustal reworking (Biswal & Sinha, 2004; Chetty & Murthy, 1994; Singh & Mishra, 2002). Geochronological studies suggest that the EGMB underwent significant tectonothermal events during the Mesoproterozoic and Neoproterozoic, linked to the assembly of Rodinia and Gondwana (Biswal & Sinha, 2004; Chetty & Murthy, 1994; Powell et al., 1988; Singh & Mishra, 2002). Its evolution is marked by the intrusion of granitic bodies and the development of shear zones, emphasizing its role in the tectonic reconfiguration of the Indian Peninsula. The Western Ghats, a prominent feature of the peninsular landscape, is primarily composed of the Deccan Traps, a vast flood basalt province formed during the Late Cretaceous (~65 Ma) (Figure S1) (Allègre et al., 1999; Mahoney et al., 2002; Mitchell & Widdowson, 1991; Sangode et al., 2022). The traps, linked to the Reunion mantle plume, cover a significant portion of western and central India. These basaltic flows are interbedded with sedimentary layers and laterite soils, which provide critical evidence of weathering and paleoclimatic conditions during and after the volcanic episodes. The structural orientation of the Western Ghats reflects rift-flank uplift associated with the breakup of Gondwana and the subsequent opening of the Indian Ocean (Kale et al., 2017; Widdowson, 1997). Their steep western escarpments are indicative of tectonic uplift and erosional processes, while the eastern slopes grade gently into the Deccan Plateau.

The Southern Granulite Province in Tamil Nadu and Kerala is a striking metamorphic belt in Indian peninsula (Figure S1), comprising high-grade metamorphic rocks, including mafic granulites, charnockites, and khondalites. This province has been pivotal in reconstructions of East Gondwana (Dev & Tomson, 2024; Plavsa et al., 2015; Tomson & Dev, 2024). Geochronological studies indicate that granulite facies metamorphism occurred around 2.5 Ga (Plavsa et al., 2015; Tomson & Dev, 2024), followed by Pan-African reworking during the late Neoproterozoic to Cambrian periods. In northwestern part of peninsular India, the Aravalli-Banded Gneiss Complex and Bundelkhand Craton record (Figure S1) the interplay of Archaean and Proterozoic tectonics (Hahn et al., 2020; Kaur et al., 2024; Mohanty, 2023; Singh et al., 2020). The Aravalli Supergroup comprises sedimentary and volcanic sequences, which were deposited in fault-controlled basins and later deformed during Proterozoic orogenesis. The Bundelkhand Craton, dominated by granitoids and mafic dyke swarms, stabilized in the Late Archaean, serving as the basement for the Vindhyan sediments (Gokarn et al., 2013; Singh et al., 2021).

S2. Evolution of the Indian Plate tectonic setting

The 160 million years tectonic history of the Indian plate begins with its separation from the Gondwanaland in the southern hemisphere, and records a complex interplay of plate movements, interaction with mantle plumes, magmatism, and collisions with Eurasia. Its breakup from the Gondwana Supercontinent in Late Jurassic (~167 Ma) (Norton & Sclater, 1979; Raval & Veeraswamy, 2003) led to opening of a nascent ocean basin that separated East Gondwana—comprising India, Madagascar, Antarctica, and Australia from West Gondwana, comprising Africa and South America (Figure S2). This opening event initiated the Southwest Indian Ridge (SWIR) as a divergent plate boundary. By the Early Cretaceous (~130 Ma), the Indian plate separated from Antarctica and Australia, forming the Southeast Indian Ridge (SEIR) (Figure S2) (Gaina et al., 2007; Johnson et al., 1980; Powell et al., 1988; Weissel et al., 1977) . During this period, Sri Lanka also experienced limited rifting from India, but ultimately remained attached to the Indian plate (Desa et al., 2018; Katz, 2000; Ratheesh-Kumar et al., 2020). An equally critical phase in the Indian plate's tectonic evolution occurred around 70 Ma with the separation of the Laxmi Ridge (Mishra et al., 2020; Talwani & Reif, 1998). Located in the Arabian Sea, the Laxmi Ridge represents a microcontinental fragment that was initially part of the Indian plate. Its rifting and subsequent isolation were closely associated with mantle plume activity, particularly from the Reunion plume (Figure S2) (Mishra et al., 2018; Singh, 1999). The separation of the Laxmi Ridge created the Laxmi Basin, which further lengthened the western margin of the Indian plate. This tectonic reorganization also contributed to the development of the Carlsberg Ridge, a major spreading center in the Indian Ocean (Figure S2) (Bohannon et al., 1989; Dyment, 1998; Illarionov & Boyko, 2018) .

Following the rifting of Madagascar, the Indian plate entered a period of unprecedented northward acceleration, with velocities reaching up to 20 cm/year during the Late Cretaceous period (~67 Ma) (Ghosh & Sengupta, 2020; Powell et al., 1988; Raval & Veeraswamy, 2003). This rapid motion is thought to be a consequence of slab pull forces exerted by the subducting Tethyan lithosphere beneath Eurasia (Eagles & Hoang, 2014; Van Hinsbergen et al., 2011; McKenzie & Sclater, 1971; Peirce, 1978) . The plate's rapid movement coincided with one of Earth's most significant volcanic events: the eruption of the Deccan Traps around 65 Ma (Allègre et al., 1999; Mitchell & Widdowson, 1991; Sen, 2001; Watts & Cox, 1989), which is linked to the Reunion plume activities (Figure S2) (Mahoney et al., 2002; Melluso et al., 2006; O'Neill et al., 2003; Tiwari et al., 2007). As the Indian plate continued its northward migration, it encountered the Kohistan-Ladakh Arc (~85 Ma) (Burg, 2011; Clift et al., 2002; Gibbons et al., 2015; Jagoutz et al., 2019; Martin et al., 2020; Rehman et al., 2011; Sharma, 1987; J. Sun et al., 2016), a volcanic island arc system located along the southern margin of the Asian plate (Figure S2). This collision, which occurred along the Indus Suture Zone, marked the beginning of India's interaction with Eurasia. The accretion of the Kohistan-Ladakh Arc to the Indian plate reflects the progressive narrowing of the Neotethys Ocean (Figure S2) (Burg, 2011; Gibbons et al., 2015; Jagoutz et al., 2019; Martin et al., 2020; Rehman et al., 2011). The culmination of the Indian plate tectonics occurred in the Early Eocene (~50 Ma)(Burg, 2011; Khan et al., 2009; Peltzer & Tapponnier, 1988; Sharma, 1987) when it collided with the Eurasian continent, resulting in complete closure of the Tethys Ocean and the rise of the Himalaya (Flesch et al., 2001; Larson et al., 1999; Patriat & Achache, 1984; Zahirovic et al., 2012; Zheng et al., 2017) . At this stage the northward velocity reduced to about 5 cm/year (Flesch et al., 2001; Patriat & Achache, 1984; Zahirovic et al., 2012). As the convergence continued during 21 Ma to the present (Larson et al., 1999; Zheng et al., 2017), the foreland basins and thrust belts characteristic of the present-day Himalayas began to take shape.

The formation of the Bay of Bengal can be traced back to the Late Jurassic and Early Cretaceous (~160–130 Ma) during the fragmentation of Gondwana (Biswas & Majumdar, 1997; Curray & Moore, 1974; Rao et al., 1997; Talwani et al., 2016) . The rifting between East and West Gondwana marked the initiation phase of this ocean basin (Figure S2) (Krishna et al., 2009; Mukherjee et al., 2009; Ramana et al., 1994) . This process was facilitated by the activation of the Southeast Indian Ridge (SEIR) (Figure S2), which began spreading and creating the Indian Ocean (Biswal & Sinha, 2004; Gaina et al., 2007; K. S. Krishna et al., 2009). During this time, the eastern margin of the Indian plate evolved as a passive continental margin, experiencing significant extensional tectonics and lithospheric thinning. As the plate moved, the eastern margin of the Indian subcontinent became a major depositional site, capturing massive volumes of sediment transported by ancient river systems such as the paleo-Ganges and paleo-Brahmaputra (Curray & Moore, 1974; P. K. Mohanty et al., 2008; Mukhopadhyay et al., 2010; Rao et al., 1997). These sediments were derived from the weathering of Gondwana terrains and volcanic materials, resulting in extensive sedimentary sequences along the margin.

The Indian plate's ongoing subduction beneath the Burma microplate led to the formation of accretionary prisms, deep-sea trenches, and active fault systems, creating a complex tectonic and depositional environment in the eastern Bay of Bengal. The tectonic evolution of the Bay of Bengal is also linked to the dynamics of the Ninety East Ridge, a prominent submarine feature extending north-south through the Bay (Figure S2) (Kolluru S. Krishna et al., 2012; Levchenko et al., 2021; Mahoney et al., 1983; Nobre Silva et al., 2013; Subrahmanyam et al., 2008; Sushchevskaya et al., 2016). This ridge represents the hotspot trace of the Kerguelen plume (Figure S2), formed during the northward drift of the Indian plate. Its alignment and magmatic history provide evidence of the plate's movement and interactions with underlying mantle dynamics. The Ninety East Ridge has also acted as a barrier to sediment transport, influencing the depositional patterns within the Bay. Modern tectonic activity in the Bay of Bengal is characterized by active subduction at the Sunda Trench and strike-slip faulting along the Andaman-Nicobar Islands (Curray, 2005; Jacob et al., 2021; S. C. Singh et al., 2013). The ongoing convergence between the Indian plate and the Burma microplate contributes to seismic activity (Cochran, 2010; McCaffrey, 2009; Mohanty et al., 2024; Panda et al., 2020; Satyabala, 2003; Sloan et al., 2017), with significant implications for regional tectonics and tsunami generation.

Rifting along the Southwest Indian Ridge led to the formation of the proto-Arabian Sea, characterized by extensional tectonics and lithospheric thinning. A major tectonic phase occurred during the Late Cretaceous (~90 Ma) (Figure S2) (Ghosh & Sengupta, 2020; Raval & Veeraswamy, 2003) when the Indian plate rifted from Madagascar, creating the Mascarene Basin and marking the initiation of the Laxmi Ridge as a distinct microcontinental fragment (Pandey et al., 1995; Talwani & Reif, 1998). The Marion mantle plume (Figure S2) is held responsible for this separation, triggering volcanism and shaping tectonic structures. such as the Laxmi Basin (Mishra et al., 2018; Pandey et al., 1995; A. P. Singh, 1999). By ~70 Ma, the Reunion mantle plume activated, causing the separation of the Laxmi Ridge from the Indian plate and initiating seafloor spreading at the Carlsberg Ridge, which continued to remain an active mid-ocean ridge in the Present day (Figure S2). The eruption of the Deccan Traps (~65 Ma), associated with this plume, profoundly influenced the region, contributing volcanic material to the Arabian Sea and aiding in the rapid northward drift of the Indian plate (Mitchell & Widdowson, 1991; Sangode et al., 2022; Watts & Cox, 1989).The collision of the Indian plate with Eurasia in the Early Eocene (~50 Ma) reshaped the northern Arabian Sea margins (Figure S2), forming subduction at the Makran Trench. Concurrently, the Owen Fracture Zone emerged as a major transform fault (Figure S2), delineating the boundary between the Indian and Arabian plates and adding complexity to the region's tectonic framework.

S3. Topographic slope calculation for Indian Peninsula (IP) topography using first-order polynomial Fit

To calculate the topographic slope along a given, transect in the peninsular terrain, we use a first-order polynomial fit to the elevation data obtained from the corresponding digital elevation maps (DEM). This method ensures accurate quantification of the first-order topographic slope from a linear regression, which captures the general inclination of the landscape by filtering out higher-order (local) topographic fluctuations. The elevation profile in peninsular topography is expressed as:

$$z = mx + c \tag{s.1}$$

where z represents elevation, x is the horizontal distance, $m$is the slope (rate of elevation change with respect to distance), and c is the intercept, representing the elevation where the horizontal distance x is zero. The slope, m, is the primary parameter of interest as it quantifies the steepness of the terrain. Using the least-squares method, the slope m is determined by minimizing the sum of squared residuals between observed elevations and those predicted by the polynomial model. The least-squares solution for m is given by:

$$m = \frac{\sum x_i z_i - \sum x_i \sum z_i}{n \sum x_i^2 - (\sum x_i)^2} \tag{s.2}$$

Here, n is the total number of data points, $\sum x_i$is the sum of horizontal distances, $\sum z_i$is the sum of elevation values, $\sum x_i \sum z_i$ is the sum of the products of distances and elevations, and $\sum {x_i}^2$ is the sum of squared distances. The intercept c can be subsequently computed as:

$$c = \frac{\sum z_i - m \sum x_i}{n} \qquad \text{(s.3)}$$

In peninsular topography, a transect often spans across gently sloping plateaus, dissected river valleys, or escarpments, which are characteristic features of such landscapes. The slope derived from this method provides a representative measure of the terrain's inclination, capturing the overall topographic trend. The polynomial fitting process is implemented in MATLAB, a computational environment that efficiently handles matrix operations and performs least-squares regression (Kiusalaas, 2015; Chen et al., 2005). The input data comprise horizontal distances x_i and corresponding elevation values $z_i$sampled along transects from digital elevation models (DEMs) of peninsular regions. The derived slope values were cross-validated against known geological gradients to ensure consistency and reliability.

The application of a first-order polynomial fit to peninsular topography provides several advantages. It allows for the simplification of complex terrain into a linear model that is easy to interpret and compare across regions. Moreover, it highlights larger-scale topographic trends that are crucial for understanding geological processes such as erosion, sediment transport, and tectonic uplift. By focusing on the overall slope, the method effectively excludes local topographic gradients due to various geomorphic elements, such as minor ridges and valleys, which are not important in the present topographic analysis.

S4. Modelling strategy

The present modelling approach simplifies the geodynamic setting of the Indian Plate (IP) by excluding additional tectonic factors, such as the northward motion of the Indian plate, far-field effects from the Sumatra Trench subduction zone, and the synkinematic infilling of sediments in ocean basins. While this simplification aids in model tractability, it limits the quantitative accuracy of the results. Moreover, the current 2D model assumes that gravity-driven sublithospheric mantle flows occur entirely within east-west (E-W) vertical planes, with minimal or no north-south (N-S) flow components. However, seismic anisotropy reveals significant azimuthal variations in mantle flow (*cf.* Figure 11b), suggesting directional variability that is not captured in this 2D framework. Consequently, the effects of non-planar mantle flows remain unaddressed in the current model. To address this limitation, future studies would benefit from incorporating 3D modeling to capture the full complexity of mantle dynamics. In our model, the Indian continental lithosphere is represented as a two-layer continuum using a thin-sheet approximation. This simplification reduces computational complexity but does not account for smaller-scale heterogeneities that may play a significant role in localized tectonic and geomorphological processes (Kale et al., 2017; Kumar et al., 2013; G. K. Saha et al., 2020). Despite this, the model provides valuable insights into the first-order topographic features of the Indian Peninsula, which appear to be primarily shaped by large-scale sublithospheric mantle flows. The main objective of this study is to explore the dynamics responsible for the eastward tilting of the Indian Peninsular topography. To achieve this, we focused on a relatively short time span, sufficient to capture the immediate lithospheric and mantle responses to tectonic and gravitational forces. This approach allows us to identify the specific mechanisms responsible for the observed topographic slopes.

References

Allègre, C. J., Birck, J. L., Capmas, F., & Courtillot, V. (1999). Age of the Deccan traps using 187Re–187Os systematics. *Earth and Planetary Science Letters*, *170*(3), 197–204. https://doi.org/10.1016/S0012-821X(99)00110-7

Amal Dev, J., & Tomson, J. K. (2024). U-Pb geochronology of rutiles from Southern granulite Terrane, India: Implications for the cooling and exhumation of East Gondwanan terranes. *Precambrian Research*, *407*, 107408. https://doi.org/10.1016/J.PRECAMRES.2024.107408

Biswal, T. K., & Sinha, S. (2004). Fold-Thrust-Belt Structure of the Proterozoic Eastern Ghats Mobile Belt: A Proposed Correlation Between India and Antarctica in Gondwana. *Gondwana Research*, *7*(1), 43–56. https://doi.org/10.1016/S1342-937X(05)70305-1

Biswas, S., & Majumdar, R. K. (1997). Seismicity and tectonics of the Bay of Bengal: Evidence for intraplate deformation of the northern Indian plate. *Tectonophysics*, *269*(3–4), 323–336. https://doi.org/10.1016/S0040-1951(96)00168-0

Bohannon, R. G., Naeser, C. W., Schmidt, D. L., & Zimmermann, R. A. (1989). The timing of uplift, volcanism, and rifting peripheral to the Red Sea: A case for passive rifting? *Journal of Geophysical Research: Solid Earth*, *94*(B2), 1683–1701. https://doi.org/10.1029/JB094IB02P01683

Boraiaha, C. K. (2022). Geochemistry of the Precambrian mafic dykes in and around the Western Ghats greenstone belt, Western Dharwar Craton. *Journal of Earth System Science*, *131*(2), 1–19. https://doi.org/10.1007/S12040-022-01865-6/FIGURES/8

Bose, P. K., Sarkar, S., Das, N. G., Banerjee, S., Mandal, A., & Chakraborty, N. (2015). Proterozoic Vindhyan Basin: Configuration and evolution. *Geological Society Memoir*, *43*, 85–102. https://doi.org/10.1144/M43.6

Burg, J. P. (2011). The Asia–Kohistan–India Collision: Review and Discussion. *Frontiers in Earth Sciences*, *4*, 279–309. https://doi.org/10.1007/978-3-540-88558-0_10

Chadwick, B., Vasudev, V. N., & Hegde, G. V. (2000). The Dharwar craton, southern India, interpreted as the result of Late Archaean oblique convergence. *Precambrian Research*, *99*(1–2), 91–111. https://doi.org/10.1016/S0301-9268(99)00055-8

Chadwick, Brian, Vasudev, V. N., & Hegde, G. V. (1997). The dharwar craton, southern india, and its late archaean plate tectonic setting: current interpretations and controversies. *Proceedings of the Indian Academy of Sciences, Earth and Planetary Sciences*, *106*(4), 249–258. https://doi.org/10.1007/BF02843452

Chatterjee, S., Goswami, A., & Scotese, C. R. (2013). The longest voyage: Tectonic, magmatic, and paleoclimatic evolution of the Indian plate during its northward flight from Gondwana to Asia. *Gondwana Research*, *23*(1), 238–267. https://doi.org/10.1016/J.GR.2012.07.001

Chetty, T. R. K., & Murthy, D. S. N. (1994). Collision tectonics in the late Precambrian Eastern Ghats Mobile Belt: mesoscopic to satellite-scale structural observations. *Terra Nova*, *6*(1), 72–81. https://doi.org/10.1111/J.1365-3121.1994.TB00635.X

Clift, P. D., Hannigan, R., Blusztajn, J., & Draut, A. E. (2002). Geochemical evolution of the Dras–Kohistan Arc during collision with Eurasia: Evidence from the Ladakh Himalaya, India. *Island Arc*, *11*(4), 255–273. https://doi.org/10.1046/J.1440-1738.2002.00371.X

Cochran, J. R. (2010). Morphology and tectonics of the Andaman Forearc, northeastern Indian Ocean. *Geophysical Journal International*, *182*(2), 631–651. https://doi.org/10.1111/J.1365-246X.2010.04663.X/2/182-2-631-FIG018.JPEG

Curray, J. R. (2005). Tectonics and history of the Andaman Sea region. *Journal of Asian Earth Sciences*, *25*(1), 187–232. https://doi.org/10.1016/J.JSEAES.2004.09.001

Curray, J. R., & Moore, D. G. (1974). Sedimentary and Tectonic Processes in the Bengal Deep-Sea Fan and Geosyncline. *The Geology of Continental Margins*, 617–627. https://doi.org/10.1007/978-3-662-01141-6_45

Desa, M. A., Ismaiel, M., Suresh, Y., & Krishna, K. S. (2018). Oblique strike-slip motion off the Southeastern Continental Margin of India: Implication for the separation of Sri Lanka from India. *Journal of Asian Earth Sciences*, *156*, 111–121. https://doi.org/10.1016/J.JSEAES.2018.01.015

Dey, S., & Moyen, J. F. (2020). Archean granitoids of India: Windows into early earth tectonics – an introduction. *Geological Society Special Publication*, *489*(1), 1–13. https://doi.org/10.1144/SP489-2020-155/ASSET/77FD8629-9782-4093-B89C-02A1EBEB23BE/ASSETS/GRAPHIC/01_GSLSPECPUB2020-155F04.JPEG

Dyment, J. (1998). Evolution of the Carlsberg Ridge between 60 and 45 Ma: Ridge propagation, spreading asymmetry, and the Deccan-Reunion hotspot. *Journal of Geophysical Research: Solid Earth*, *103*(B10), 24067–24084. https://doi.org/10.1029/98JB01759

Eagles, G., & Hoang, H. H. (2014). Cretaceous to present kinematics of the Indian, African and Seychelles plates. *Geophysical Journal International*, *196*(1), 1–14. https://doi.org/10.1093/GJI/GGT372

Flesch, L. M., Haines, A. J., & Holt, W. E. (2001). Dynamics of the India-Eurasia collision zone. *Journal of Geophysical Research: Solid Earth*, *106*(B8), 16435–16460. https://doi.org/10.1029/2001JB000208

Gaina, C., Müller, R. D., Brown, B., Ishihara, T., & Ivanov, S. (2007). Breakup and early seafloor spreading between India and Antarctica. *Geophysical Journal International*, *170*(1), 151–169. https://doi.org/10.1111/J.1365-246X.2007.03450.X/2/170-1-151-FIG011.JPEG

Ghosh, P., & Sengupta, D. P. (2020). Geodynamics of Gondwanaland. *Springer Geology*, 213–232. https://doi.org/10.1007/978-3-030-15989-4_7

Gibbons, A. D., Zahirovic, S., Müller, R. D., Whittaker, J. M., & Yatheesh, V. (2015). A tectonic model reconciling evidence for the collisions between India, Eurasia and intra-oceanic arcs of the central-eastern Tethys. *Gondwana Research*, *28*(2), 451–492. https://doi.org/10.1016/j.gr.2015.01.001

Gokarn, S. G., Rao, C. K., Selvaraj, C., & Gupta, G. (2013). Crustal evolution and tectonics of the Archean Bundelkhand craton, Central India. *Journal of the Geological Society of India*, *82*(5), 455–460. https://doi.org/10.1007/S12594-013-0176-6/METRICS

Goswami, S., Bhagat, S., Pande, D., Choudhury, D. K., Saravanan, B., & Sinha, D. K. (2023). Implication of deformation fabrics of schist-migmatite-gneiss and granite in understanding regional tectonics: Eastern Dharwar Craton (EDC), India. *Proceedings of the Indian National Science Academy*, *89*(3), 613–643. https://doi.org/10.1007/S43538-023-00173-X/METRICS

Hahn, G., Kodl, G., de Wall, H., Schulz, B., Bestmann, M., & Chauhan, N. K. (2020). Deformation in the Aravalli Supergroup, Aravalli-Delhi Mobile Belt, NW India and Tectonic Significance, 23–55. https://doi.org/10.1007/978-3-030-40593-9_2

Van Hinsbergen, D. J. J., Steinberger, B., Doubrovine, P. V., & Gassmöller, R. (2011). Acceleration and deceleration of India-Asia convergence since the Cretaceous: Roles of mantle plumes and continental collision. *Journal of Geophysical Research: Solid Earth*, *116*(B6). https://doi.org/10.1029/2010JB008051

Hofmann, A., Jodder, J., Xie, H., Bolhar, R., Whitehouse, M., & Elburg, M. (2022). The Archaean geological history of the Singhbhum Craton, India – a proposal for a consistent framework of craton evolution. *Earth-Science Reviews*, *228*, 103994. https://doi.org/10.1016/J.EARSCIREV.2022.103994

Illarionov, V. K., & Boyko, A. N. (2018). Geodynamic Aspects of the Evolution of the Northwestern Indian Ocean. *Izvestiya - Atmospheric and Ocean Physics*, *54*(7), 768–776. https://doi.org/10.1134/S0001433818070034/FIGURES/3

Jacob, J., Dyment, J., Ghosal, D., & Dewangan, P. (2021). Strike-slip seismicity at the Andaman-Sumatra Subduction Zone: Role of the fracture zones and age of the subducting lithosphere. *Tectonophysics*, *811*, 228862. https://doi.org/10.1016/J.TECTO.2021.228862

Jagoutz, O., Bouilhol, P., Schaltegger, U. R. S., & Müntener, O. (2019). The isotopic evolution of the Kohistan Ladakh arc from subduction initiation to continent arc collision. *Geological Society Special Publication*, *483*(1), 165–182. https://doi.org/10.1144/SP483.7

Jayananda, M., Dey, S., & Aadhiseshan, K. R. (2020). Evolving Early Earth: Insights from Peninsular India. *Springer Geology*, 5–103. https://doi.org/10.1007/978-3-030-15989-4_2

Jayananda, M., Guitreau, M., Aadhiseshan, K. R., Miyazaki, T., & Chung, S. L. (2023). Origin of the oldest (3600–3200 Ma) cratonic core in the Western Dharwar Craton, Southern India: Implications for evolving tectonics of the Archean Earth. *Earth-Science Reviews*, *236*, 104278. https://doi.org/10.1016/J.EARSCIREV.2022.104278

Johnson, B. D., Powell, C. M. A., & Veevers, J. J. (1980). Early spreading history of the Indian Ocean between India and Australia. *Earth and Planetary Science Letters*, *47*(1), 131–143. https://doi.org/10.1016/0012-821X(80)90112-0

Kale, V. S., Dole, G., Upasani, D., & Pillai, S. P. (2017). Deccan plateau uplift: Insights from parts of western uplands, Maharashtra, India. *Geological Society Special Publication*, *445*(1), 11–46. https://doi.org/10.1144/SP445.2/ASSET/AC944E2D-CDFF-4081-9DE7-9281E74175EF/ASSETS/GRAPHIC/SP445-1505F14.JPEG

Katz, M. B. (2000). Sri Lanka - India Intraplate Tectonics - Precambrian to Present. *Gondwana Research*, *3*(1), 3–5. https://doi.org/10.1016/S1342-937X(05)70052-6

Kaur, P., Chaudhri, N., Saha, L., & Nasipuri, P. (2024). Crustal evolution of the Aravalli and Bundelkhand Archean nuclei, North Indian Block: recent advances and perspectives. *Proceedings of the Indian National Science Academy*, *90*(2), 196–208. https://doi.org/10.1007/S43538-024-00278-X/METRICS

Khan, S. D., Walker, D. J., Hall, S. A., Burke, K. C., Shah, M. T., & Stockli, L. (2009). Did the Kohistan-Ladakh island arc collide first with India? *GSA Bulletin*, *121*(3–4), 366–384. https://doi.org/10.1130/B26348.1

Kiusalaas, J. (2015). Numerical Methods in Engineering with MATLAB®. *Numerical Methods in Engineering with MATLAB®*. https://doi.org/10.1017/CBO9781316341599

Krapež, B., Srinivasa Sarma, D., Ram Mohan, M., McNaughton, N. J., Rasmussen, B., & Wilde, S. A. (2020). Tectonostratigraphy of the Late Archean Dharwar Supergroup, Dharwar Craton, India: Defining a tectonic history from spatially linked but temporally distinct intracontinental and arc-related basins. *Earth-Science Reviews*, *201*. https://doi.org/10.1016/J.EARSCIREV.2019.102966b

Krishna, K. S., Michael, L., Bhattacharyya, R., & Majumdar, T. J. (2009). Geoid and gravity anomaly data of conjugate regions of Bay of Bengal and Enderby Basin: New constraints on breakup and early spreading history between India and Antarctica. *Journal of Geophysical Research: Solid Earth*, *114*(B3). https://doi.org/10.1029/2008JB005808

Krishna, Kolluru S., Abraham, H., Sager, W. W., Pringle, M. S., Frey, F., Gopala Rao, D., & Levchenko, O. V. (2012). Tectonics of the Ninetyeast Ridge derived from spreading records in adjacent oceanic basins and age constraints of the ridge. *Journal of Geophysical Research: Solid Earth*, *117*(B4). https://doi.org/10.1029/2011JB008805

Kumar, M. R., Saikia, D., Singh, A., Srinagesh, D., Baidya, P. R., & Dattatrayam, R. S. (2013). Low shear velocities in the sub-lithospheric mantle beneath the Indian shield? *Journal of Geophysical Research: Solid Earth*, *118*(3), 1142–1155. https://doi.org/10.1002/JGRB.50114

Larson, K. M., Bürgmann, R., Bilham, R., & Freymueller, J. T. (1999). Kinematics of the India-Eurasia collision zone from GPS measurements. *Journal of Geophysical Research: Solid Earth*, *104*(B1), 1077–1093. https://doi.org/10.1029/1998JB900043

Levchenko, O. V., Sushchevskaya, N. M., & Marinova, Y. G. (2021). The Nature and Evolution of the Ninetyeast Ridge: A Key Tectonic and Magmatic Feature of the East Indian Ocean. *Geotectonics*, *55*(2), 194–218. https://doi.org/10.1134/S0016852121020060/FIGURES/9

Mahoney, J. J., Macdougall, J. D., Lugmair, G. W., & Gopalan, K. (1983). Kerguelen hotspot source for Rajmahal Traps and Ninetyeast Ridge? *Nature 1983 303:5916*, *303*(5916), 385–389. https://doi.org/10.1038/303385a0

Mahoney, J. J., Duncan, R. A., Khan, W., Gnos, E., & McCormick, G. R. (2002). Cretaceous volcanic rocks of the South Tethyan suture zone, Pakistan: implications for the Réunion hotspot and Deccan Traps. *Earth and Planetary Science Letters*, *203*(1), 295–310. https://doi.org/10.1016/S0012-821X(02)00840-3

Martin, C. R., Jagoutz, O., Upadhyay, R., Royden, L. H., Eddy, M. P., Bailey, E., et al. (2020). Paleocene latitude of the Kohistan-Ladakh arc indicates multistage India-Eurasia collision. *Proceedings of the National Academy of Sciences of the United States of America*, *117*(47), 29487–29494. https://doi.org/10.1073/PNAS.2009039117/SUPPL_FILE/PNAS.2009039117.SD01.XLSX

McCaffrey, R. (2009). The tectonic framework of the sumatran subduction zone. *Annual Review of Earth and Planetary Sciences*, *37*(Volume 37, 2009), 345–366. https://doi.org/10.1146/ANNUREV.EARTH.031208.100212/CITE/REFWORKS

McKenzie, D., & Sclater, J. G. (1971). The Evolution of the Indian Ocean since the Late Cretaceous. *Geophysical Journal International*, *24*(5), 437–528. https://doi.org/10.1111/J.1365-246X.1971.TB02190.X

Meert, J.G., & Pandit, M.K. (2015). The Archean and Proterozoic history of Peninsular India: Tectonic framework for Precambrian sedimentary basin in India. *Geological Society, London, Memoirs*, no.1 (2015): 29-54

Melluso, L., Mahoney, J. J., & Dallai, L. (2006). Mantle sources and crustal input as recorded in high-Mg Deccan Traps basalts of Gujarat (India). *Lithos*, *89*(3–4), 259–274. https://doi.org/10.1016/J.LITHOS.2005.12.007

Miall, A. D., Catuneanu, O., Eriksson, P. G., & Mazumder, R. (2015). A brief synthesis of Indian Precambrian basins: Classification and genesis of basin-fills. *Geological Society Memoir*, *43*, 339–347. https://doi.org/10.1144/M43.23

Mishra, A., Chaubey, A. K., Sreejith, K. M., & Kumar, S. (2018). Crustal underplating and effective elastic plate thickness of the Laxmi Ridge, northern Arabian Sea. *Tectonophysics*, *744*, 82–92. https://doi.org/10.1016/J.TECTO.2018.06.013

Mishra, A., Chaubey, A. K., Kumar, S., Kumar, P. V., Kumar, P., & Dubey, K. M. (2020). Does the Laxmi Ridge continue towards the Laccadive Ridge? New insights from an integrated geophysical study. *Journal of Asian Earth Sciences*, *201*, 104491. https://doi.org/10.1016/J.JSEAES.2020.104491

Mitchell, C., & Widdowson, M. (1991). A geological map of the southern Deccan Traps, India and its structural implications. *Journal of the Geological Society*, *148*(3), 495–505. https://doi.org/10.1144/GSJGS.148.3.0495

Mohan, M. R., Piercey, S. J., Kamber, B. S., & Sarma, D. S. (2013). Subduction related tectonic evolution of the Neoarchean eastern Dharwar Craton, southern India: New geochemical and isotopic constraints. *Precambrian Research*, *227*, 204–226. https://doi.org/10.1016/J.PRECAMRES.2012.06.012

Mohan, M. R., Asokan, A. D., & Wilde, S. A. (2020). Crustal growth of the eastern dharwar craton: A neoarchean collisional orogeny? *Geological Society Special Publication*, *489*(1), 51–77. https://doi.org/10.1144/SP489-2019-108

Mohanty, D. D., Biswal, S., & Yoshizawa, K. (2024). Decoupled deformation between crust and mantle beneath Indo-Burmese Wedge: A new seismotectonic model. *Earth and Planetary Science Letters*, *648*, 119089. https://doi.org/10.1016/J.EPSL.2024.119089

Mohanty, P. K., Pradhan, Y., Nayak, S. R., Panda, U. S., & Mohapatra, G. N. (2008). Sediment Dispersion in the Bay of Bengal. *Monitoring and Modelling Lakes and Coastal Environments*, 50–78. https://doi.org/10.1007/978-1-4020-6646-7_5

Mohanty, S. P. (2021). The Bastar Craton of Central India: Tectonostratigraphic evolution and implications in global correlations. *Earth-Science Reviews*, *221*, 103770. https://doi.org/10.1016/J.EARSCIREV.2021.103770

Mohanty, S. P. (2023). Proterozoic basins of the Bundelkhand Craton, India: Correlations and significance in understanding the tectonic evolution. *Geosystems and Geoenvironment*, *2*(2), 100155. https://doi.org/10.1016/J.GEOGEO.2022.100155

Mondal, M. E. A., Hussain, M. F., & Ahmad, T. (2006). Continental growth of Bastar craton, central Indian shield during precambrian via multiphase subduction and lithospheric extension/rifting: evidence from geochemistry of gneisses, granitoids and mafic dykes. Retrieved from http://dlisv03.media.osaka-cu.ac.jp/infolib/user_contents/kiyo/DBe0490008.pdf

Mukherjee, A., Fryar, A. E., & Thomas, W. A. (2009). Geologic, geomorphic and hydrologic framework and evolution of the Bengal basin, India and Bangladesh. *Journal of Asian Earth Sciences*, *34*(3), 227–244. https://doi.org/10.1016/J.JSEAES.2008.05.011

Mukhopadhyay, G., Mukhopadhyay, S. K., Roychowdhury, M., & Parui, P. K. (2010). Stratigraphic correlation between different Gondwana Basins of India. *Journal of the Geological Society of India*, *76*(3), 251–266. https://doi.org/10.1007/S12594-010-0097-6/METRICS

Nobre Silva, I. G., Weis, D., Scoates, J. S., & Barling, J. (2013). The Ninetyeast Ridge and its Relation to the Kerguelen, Amsterdam and St. Paul Hotspots in the Indian Ocean. *Journal of Petrology*, *54*(6), 1177–1210. https://doi.org/10.1093/PETROLOGY/EGT009

Norton, I. O., & Sclater, J. G. (1979). A model for the evolution of the Indian Ocean and the breakup of Gondwanaland. *Journal of Geophysical Research: Solid Earth*, *84*(B12), 6803–6830. https://doi.org/10.1029/JB084IB12P06803

O'Neill, C., Müller, D., & Steinberger, B. (2003). Geodynamic implications of moving Indian Ocean hotspots. *Earth and Planetary Science Letters*, *215*(1–2), 151–168. https://doi.org/10.1016/S0012-821X(03)00368-6

Panda, D., Kundu, B., Gahalaut, V. K., & Rangin, C. (2020). India-Sunda Plate Motion, Crustal Deformation, and Seismic Hazard in the Indo-Burmese Arc. *Tectonics*, *39*(8), e2019TC006034. https://doi.org/10.1029/2019TC006034

Pandey, O. P., Agrawal, P. K., & Negi, J. G. (1995). Lithospheric structure beneath Laxmi Ridge and late Cretaceous geodynamic events. *Geo-Marine Letters*, *15*(2), 85–91. https://doi.org/10.1007/BF01275411/METRICS

Patriat, P., & Achache, J. (1984). India–Eurasia collision chronology has implications for crustal shortening and driving mechanism of plates. *Nature 1984 311:5987*, *311*(5987), 615–621. https://doi.org/10.1038/311615a0

Peirce, J. W. (1978). The northward motion of India since the Late Cretaceous. *Geophysical Journal International*, *52*(2), 277–311. https://doi.org/10.1111/J.1365-246X.1978.TB04234.X

Peltzer, G., & Tapponnier, P. (1988). Formation and evolution of strike-slip faults, rifts, and basins during the India-Asia Collision: An experimental approach. *Journal of Geophysical Research: Solid Earth*, *93*(B12), 15085–15117. https://doi.org/10.1029/JB093IB12P15085

Plavsa, D., Collins, A. S., Foden, J. D., & Clark, C. (2015). The evolution of a Gondwanan collisional orogen: A structural and geochronological appraisal from the Southern Granulite Terrane, South India. *Tectonics*, *34*(5), 820–857. https://doi.org/10.1002/2014TC003706

Powell, C. M. A., Roots, S. R., & Veevers, J. J. (1988). Pre-breakup continental extension in East Gondwanaland and the early opening of the eastern Indian Ocean. *Tectonophysics*, *155*(1–4), 261–283. https://doi.org/10.1016/0040-1951(88)90269-7

Prabhakar, B. C., Jayananda, M., Shareef, M., & Kano, T. (2009). Petrology and geochemistry of late archaean granitoids in the northern part of Eastern Dharwar Craton, Southern India: Implications for transitional geodynamic setting. *Journal of the Geological Society of India*, *74*(3), 299–317. https://doi.org/10.1007/S12594-009-0137-2

Ramana, M. V., Nair, R. R., Sarma, K. V. L. N. S., Ramprasad, T., Krishna, K. S., Subrahmanyam, V., et al. (1994). Mesozoic anomalies in the Bay of Bengal. *Earth and Planetary Science Letters*, *121*(3–4), 469–475. https://doi.org/10.1016/0012-821X(94)90084-1

Ranjan, S., Upadhyay, D., Abhinay, K., & Srikantappa, C. (2020). Paleoarchean and Neoarchean Tonalite–Trondhjemite–Granodiorite (TTG) and granite magmatism in the Western Dharwar Craton, southern India: Implications for Archean continental growth and geodynamics. *Precambrian Research*, *340*. https://doi.org/10.1016/J.PRECAMRES.2020.105630

Rao, D. G., Krishna, K. S., & Sar, D. (1997). Crustal evolution and sedimentation history of the Bay of Bengal since the Cretaceous. *Journal of Geophysical Research: Solid Earth*, *102*(B8), 17747–17768. https://doi.org/10.1029/96JB01339

Ratheesh-Kumar, R. T., Dharmapriya, P. L., Windley, B. F., Xiao, W. J., & Jeevan, U. (2020). The Tectonic "Umbilical Cord" Linking India and Sri Lanka and the Tale of their Failed Rift. *Journal of Geophysical Research: Solid Earth*, *125*(5), e2019JB018225. https://doi.org/10.1029/2019JB018225

Raval, U., & Veeraswamy, K. (2003). India-Madagascar Separation: Breakup Along a Pre-existing Mobile Belt and Chipping of the Craton. *Gondwana Research*, *6*(3), 467–485. https://doi.org/10.1016/S1342-937X(05)70999-0

Rehman, H. U., Seno, T., Yamamoto, H., & Khan, T. (2011). Timing of collision of the Kohistan–Ladakh Arc with India and Asia: Debate. *Island Arc*, *20*(3), 308–328. https://doi.org/10.1111/J.1440-1738.2011.00774.X

Saha, D., & Mazumder, R. (2012). An overview of the Palaeoproterozoic geology of Peninsular India, and key stratigraphic and tectonic issues. *Geological Society Special Publication*, *365*(1), 5–29. https://doi.org/10.1144/SP365.2

Saha, D., & Patranabis-Deb, S. (2014). Proterozoic evolution of Eastern Dharwar and Bastar cratons, India – An overview of the intracratonic basins, craton margins and mobile belts. *Journal of Asian Earth Sciences*, *91*, 230–251. https://doi.org/10.1016/J.JSEAES.2013.09.020

Saha, G. K., Prakasam, K. S., & Rai, S. S. (2020). Diversity in the peninsular Indian lithosphere revealed from ambient noise and earthquake tomography. *Physics of the Earth and Planetary Interiors*, *306*, 106523. https://doi.org/10.1016/J.PEPI.2020.106523

Sangode, S. J., Dongre, A., Bhagat, A., & Meshram, D. (2022). Palaeomagnetic inclination anomaly in the Deccan traps and its geodynamic implications over the Indian plate. *Journal of Earth System Science*, *131*(3), 1–12. https://doi.org/10.1007/S12040-022-01917-X/TABLES/5

Satyabala, S. P. (2003). Oblique plate convergence in the Indo-Burma (Myanmar) subduction region. *Pure and Applied Geophysics*, *160*(9), 1611–1650. https://doi.org/10.1007/S00024-003-2378-0/METRICS

Sen, G. (2001). Generation of Deccan trap magmas. *Proceedings of the Indian Academy of Sciences, Earth and Planetary Sciences*, *110*(4), 409–431. https://doi.org/10.1007/BF02702904/METRICS

Sharma, K. K. (1987). Crustal growth and two-stage India-Eurasia collision in Ladakh. *Tectonophysics*, *134*(1–3), 17–28. https://doi.org/10.1016/0040-1951(87)90246-0

Singh, A. P. (1999). The deep crustal accretion beneath the Laxmi Ridge in the northeastern Arabian Sea: the plume model again. *Journal of Geodynamics*, *27*(4–5), 609–622. https://doi.org/10.1016/S0264-3707(98)00019-2

Singh, A. P., & Mishra, D. C. (2002). Tectonosedimentary evolution of Cuddapah basin and Eastern Ghats mobile belt (India) as Proterozoic collision: gravity, seismic and geodynamic constraints. *Journal of Geodynamics*, *33*(3), 249–267. https://doi.org/10.1016/S0264-3707(01)00066-7

Singh, S. C., Moeremans, R., McArdle, J., & Johansen, K. (2013). Seismic images of the sliver strike-slip fault and back thrust in the Andaman-Nicobar region. *Journal of Geophysical Research: Solid Earth*, *118*(10), 5208–5224. https://doi.org/10.1002/JGRB.50378

Singh, V. K., Verma, S. K., Singh, P. K., Slabunov, A. I., Mishra, S., & Chaudhary, N. (2020). Archean crustal evolution of the bundelkhand craton: Evidence from granitoid magmatism. *Geological Society Special Publication*, *489*(1), 235–259. https://doi.org/10.1144/SP489-2018-72

Singh, V. K., Slabunov, A. I., Nesterova, N. S., Singh, M. M., & Bhatt, S. C. (2021). Tectonostratigraphic Terranes of the Bundelkhand Craton (Indian Shield), 155–164. https://doi.org/10.1007/978-981-16-4122-0_10

Sloan, R. A., Elliott, J. R., Searle, M. P., & Morley, C. K. (2017). Active tectonics of Myanmar and the Andaman Sea. *Geological Society Memoir*, *48*(1), 19–52. https://doi.org/10.1144/M48.2

Subrahmanyam, C., Gireesh, R., Chand, S., Raju, K. A. K., & Rao, D. G. (2008). Geophysical characteristics of the Ninetyeast Ridge–Andaman island arc/trench convergent zone. *Earth and Planetary Science Letters*, *266*(1–2), 29–45. https://doi.org/10.1016/J.EPSL.2007.10.016

Chen, G., Ren, ZL., Sun, H. (2005). Curve Fitting in Least-Square Method and Its Realization with Matlab. *Ordnance Industry Automation*.

Sun, J., Xiao, W., Windley, B. F., Ji, W., Fu, B., Wang, J., & Jin, C. (2016). Provenance change of sediment input in the northeastern foreland of Pamir related to collision of the Indian Plate with the Kohistan-Ladakh arc at around 47 Ma. *Tectonics*, *35*(2), 315–338. https://doi.org/10.1002/2015TC003974

Sushchevskaya, N. M., Levchenko, O. V., Dubinin, E. P., & Belyatsky, B. V. (2016). Ninetyeast ridge: Magmatism and geodynamics. *Geochemistry International*, *54*(3), 237–256. https://doi.org/10.1134/S001670291603006X/METRICS

Talukdar, D., Pandey, A., Chalapathi Rao, N. V., Kumar, A., Pandit, D., Belyatsky, B., & Lehmann, B. (2018). Petrology and geochemistry of the Mesoproterozoic Vattikod lamproites, Eastern Dharwar Craton, southern India: evidence for multiple enrichment of sub-continental lithospheric mantle and links with amalgamation and break-up of the Columbia supercontinent. *Contributions to Mineralogy and Petrology*, *173*(8), 1–27. https://doi.org/10.1007/S00410-018-1493-Y/FIGURES/12

Talwani, M., & Reif, C. (1998). Laxmi Ridge - A continental sliver in the Arabian Sea. *Marine Geophysical Research*, *20*(4), 259–271. https://doi.org/10.1023/A:1004674909280/METRICS

Talwani, M., Desa, M. A., Ismaiel, M., & Sree Krishna, K. (2016). The Tectonic origin of the Bay of Bengal and Bangladesh. *Journal of Geophysical Research: Solid Earth*, *121*(7), 4836–4851. https://doi.org/10.1002/2015JB012734

Tiwari, V. M., Grevemeyer, I., Singh, B., & Phipps Morgan, J. (2007). Variation of effective elastic thickness and melt production along the Deccan–Reunion hotspot track. *Earth and Planetary Science Letters*, *264*(1–2), 9–21. https://doi.org/10.1016/J.EPSL.2007.08.023

Tomson, J. K., & Dev, J. A. (2024). Tracing the crustal evolution of the Precambrian Southern Granulite terrane in East Gondwana: New insights from zircon U-Pb/Hf geochronology. *GSA Bulletin*, *136*(5–6), 2075–2096. https://doi.org/10.1130/B36777.1

Wang, M. X., Santosh, M., Jayananda, M., Yang, C. X., Thomas, T. T., & Kim, S. W. (2023). Trondhjemites from the Western Dharwar Craton, Southern India: Implications for Mesoarchean crustal growth. *Lithos*, *462–463*, 107410. https://doi.org/10.1016/J.LITHOS.2023.107410

Watts, A. B., & Cox, K. G. (1989). The Deccan Traps: an interpretation in terms of progressive lithospheric flexure in response to a migrating load. *Earth and Planetary Science Letters*, *93*(1), 85–97. https://doi.org/10.1016/0012-821X(89)90186-6

Weissel, J. K., Hayes, D. E., & Herron, E. M. (1977). Plate tectonics synthesis: The displacements between Australia, New Zealand, and Antarctica since the Late Cretaceous. *Marine Geology*, *25*(1–3), 231–277. https://doi.org/10.1016/0025-3227(77)90054-8

Widdowson, M. (1997). Tertiary palaeosurfaces of the SW Deccan, Western India: Implications for passive margin uplift. *Geological Society Special Publication*, *120*, 221–248. https://doi.org/10.1144/GSL.SP.1997.120.01.15

Zahirovic, S., Mller, R. D., Seton, M., Flament, N., Gurnis, M., & Whittaker, J. (2012). Insights on the kinematics of the India-Eurasia collision from global geodynamic models. *Geochemistry, Geophysics, Geosystems*, *13*(4). https://doi.org/10.1029/2011GC003883

Zheng, G., Wang, H., Wright, T. J., Lou, Y., Zhang, R., Zhang, W., et al. (2017). Crustal Deformation in the India-Eurasia Collision Zone From 25 Years of GPS Measurements. *Journal of Geophysical Research: Solid Earth*, *122*(11), 9290–9312. https://doi.org/10.1002/2017JB014465

Figure S1

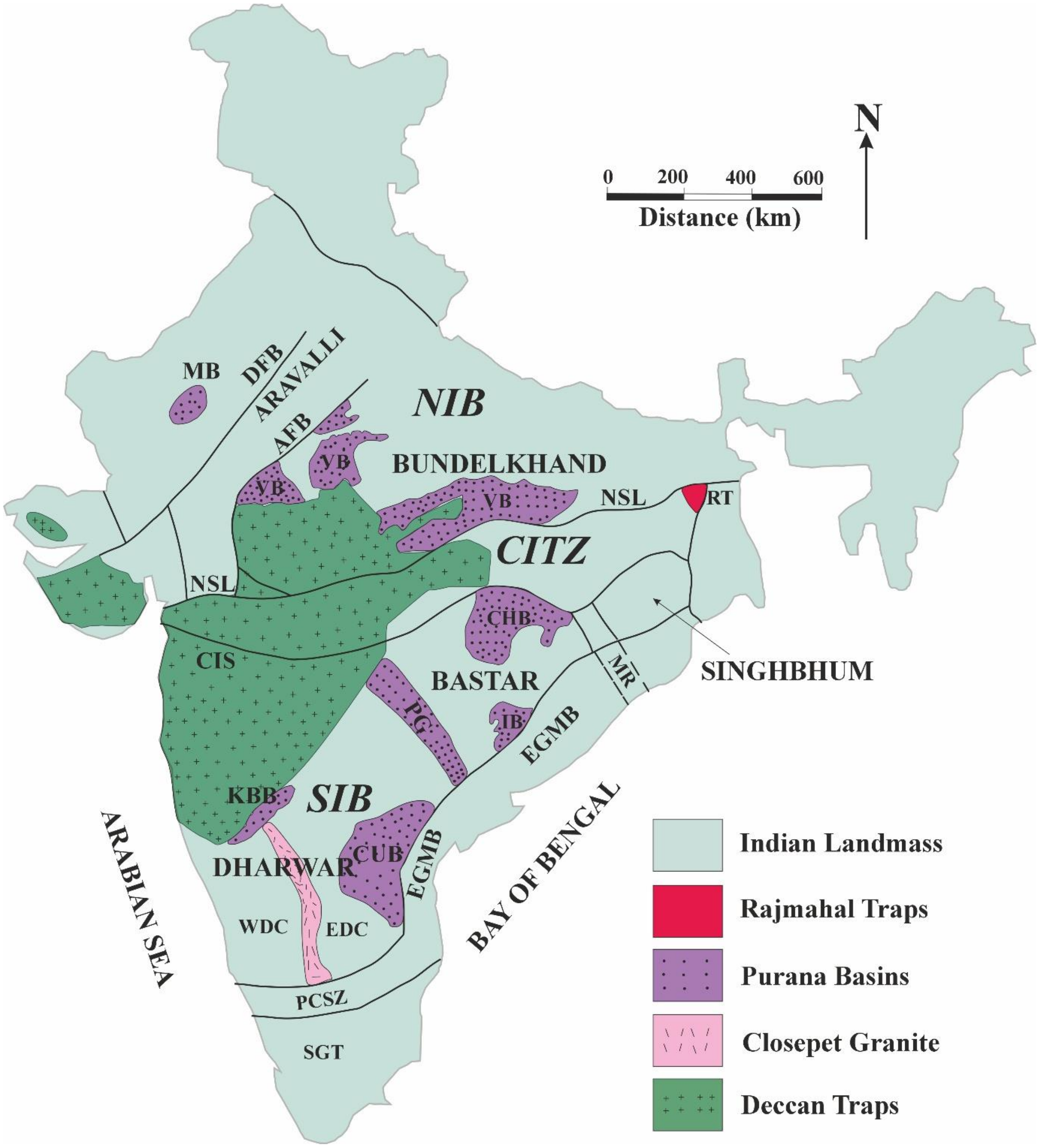

Figure S1 A simplified geological map (Meert & Pandit, 2015) of Peninsular India (IP) showing major Precambrian cratons, Proterozoic mobile belts, Sedimentary basins and Volcanic provenances. The abbreviation are as follows- NIB: North Indian Block; SIB: South

Indian Block; AFB: Aravalli Fold Belt; DFB: Delhi Fold Belt; EGMB: Eastern Ghat Mobile Belt; SMB: Satpura Mobile Belt; NSL: Narmada Son Lineament; CIS: Central Indian Suture; PCSZ: Palghat-Cauvery Shear Zone; DT: Deccan Traps; RT: Rajmahal Trap; IB: Indravati Basin; MB: Marwar Basin; VB: Vindhyan Basin; PG: Pranhita-Godavari Basin; CUB: Cuddapah Basin; KBB: Kaladgi-Bhima Basin; CHB: Chhattisgarh Basin; EDC: Eastern Dharwar Craton; WDC: Western Dharwar Craton; SGT: Southern Garnulites Terrain.

630 **Figure S2**

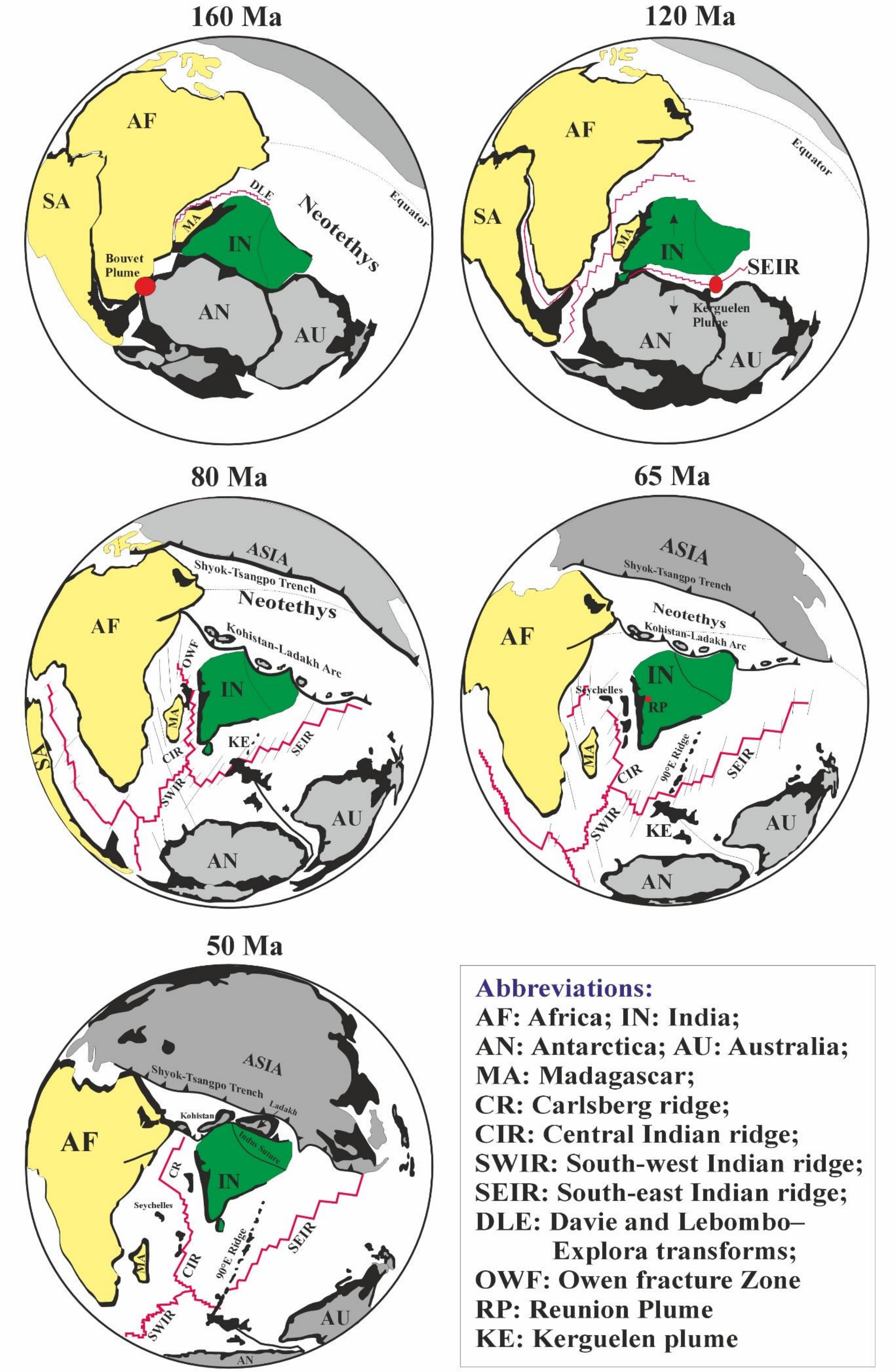

Abbreviations:
AF: Africa; IN: India;
AN: Antarctica; AU: Australia;
MA: Madagascar;
CR: Carlsberg ridge;
CIR: Central Indian ridge;
SWIR: South-west Indian ridge;
SEIR: South-east Indian ridge;
DLE: Davie and Lebombo–Explora transforms;
OWF: Owen fracture Zone
RP: Reunion Plume
KE: Kerguelen plume

Figure S2 A cartoon illustrating break-up of Gondwanaland, subsequent dispersion of the constituting continents, formation of plate boundaries and opening of the major sea from 160 Ma to 50 Ma